# Supplementary Information

**Supplementary Figure S16.** Multiple sequences alignment and secondary structural elements of alphaviruses capsid protein.

**Supplementary Figure S17.** Mass spectrometry of the N-glycosylation sites in GETV E1 protein.

**Supplementary Figure S18.** Mass spectrometry of the N-glycosylation sites in GETV E2 protein.

**Supplementary Figure S19.** Conserved glycosylation sites in the alphaviruses.

**Supplementary Figure S20.** Mass spectrometry of the S-acylation sites in the GETV E1 protein.

**Supplementary Figure S21.** Mass spectrometry of the S-acylation sites in the GETV E2 protein.

**Supplementary Figure S22.** MS spectra and table of mass shifts of S-acylation by LC-MS/MS.

**Supplementary Figure S23.** Transmembrane helices of E1 and E2.

**Supplementary Figure S24.** Time evolutions from MD simulation analyses for the native contacts within the E1-E2 complex.

**Supplementary Figure S25.** Comparison of the hydrophobic pocket between our GETV model and other alphavirus structures.

**Supplementary Table S1.** Cryo-EM data collection and processing, block-based reconstruction, model building, and refinement statistics.

**Supplementary Table S2.** Interaction areas between GETV structural proteins.

**Supplementary Table S3.** Protein-protein interactions in GETV and other alphaviruses.

**Supplementary Table S4.** Glycosylation sites in the E1 and E2 proteins.

**Supplementary Table S5.** S-acylation sites in the E1 and E2 proteins.

**Supplementary Video S1.** GETV caused mobility impairments in pelvic limbs in newborn mice.

**Supplementary Video S2.** Molecular dynamics simulation of interactions in the Wild Type E1-E2 system.

**Supplementary Video S3.** Molecular dynamics simulation of interactions in the "delCHL" (only cholesterol in the pocket was removed) system.

**Supplementary Video S4.** Molecular dynamics simulation of interactions in the "delDOPC (only DOPC in the pocket was removed) system.

**Supplementary Video S5.** Molecular dynamics simulation of interactions in the "del2CHL" (2 cholesterols surround the pocket were removed) system.

**Supplementary Video S6.** Molecular dynamics simulation of interactions in the "delCHL/DOPC" (both cholesterol and DOPC in the pocket were removed) system.

**Supplementary Video S7.** Molecular dynamics simulation of interactions in the "delALL" (all three cholesterols and DOPC were removed) system.

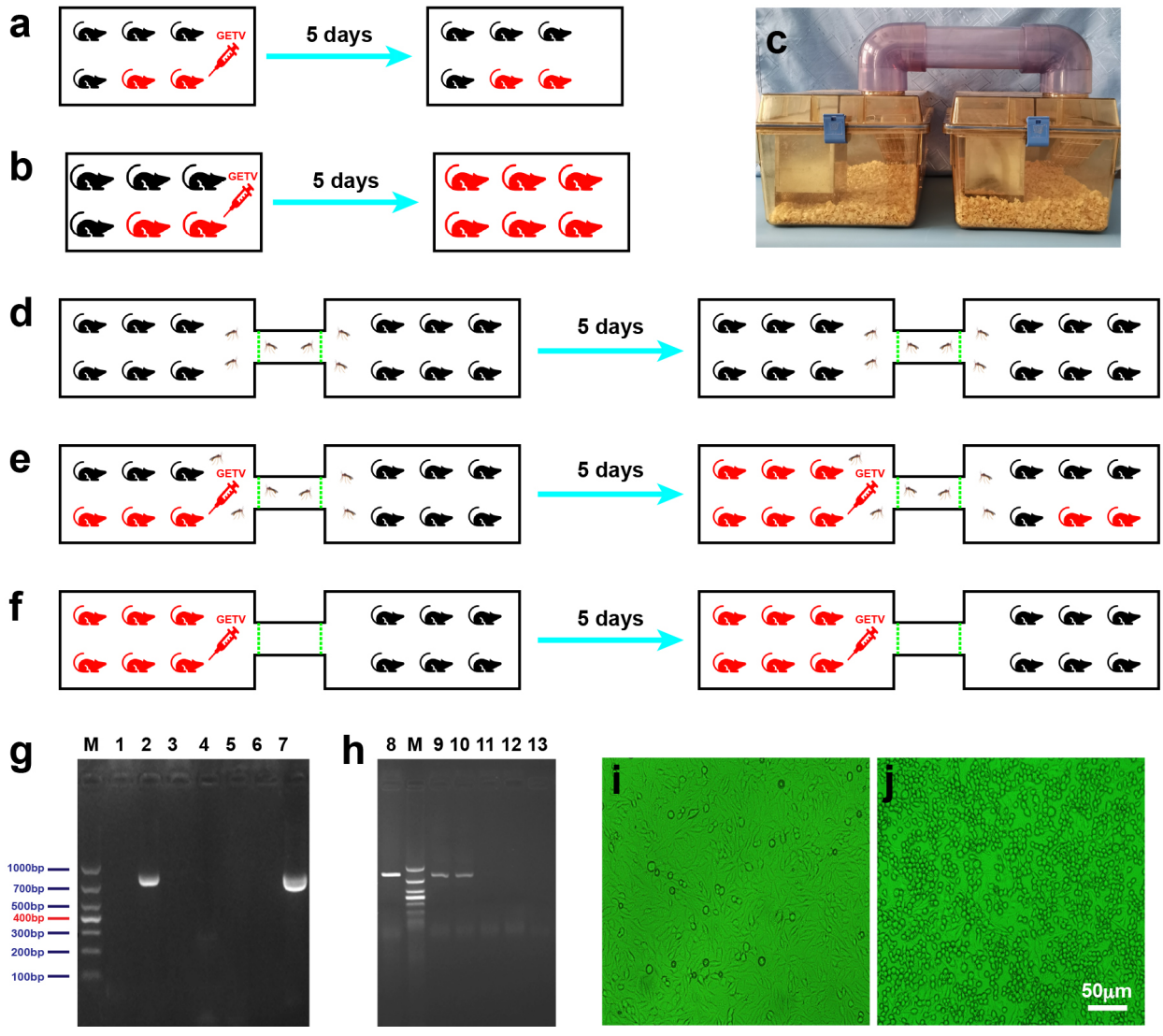


**Supplementary Figure S1. GETV is a mosquito-borne arbovirus.**

**a**, Photo of the device that was used in experiments **d** – **f**. **b** – **f**, Schematic illustrations of the experimental design to investigate the infectiousness of GETV. **b**, Experiments investigate the infectiousness of GETV between newborn mice. **c**, Experiments investigate the infectiousness of GETV between male adult mice. **d** – **f**, Experiments investigate GETV as a mosquito-borne arbovirus, not an airborne virus. **g** and **h**, Total RNA was extracted from tissue, including spleen, lung, cerebral cortex, and various lymph nodes using TRIzol reagent after 5 days post-inoculation (DPI)[1], and subjected to RT-PCR for GETV detection using specific primers (GETV-F: 5′ -

ACCGAAGAAGCCGAAGAA-3′, and GETV-R: 5′-GCACTCRAGGTCATACTTG-3′)[2]. M, markers; Lane 1, the buffer used in RT-PCR; Lane 2, supernatant of GETV cultured in BHK21 cells (positive control); Lane 3, test in mosquitos used in **d**; Lane 4 and 5, test in mice in the right-hand cage at 5 DPI in **d**; Lanes 6 and 7, GETV-free mice and infected mice in the cage at 5 DPI in **b**; Lane 8, GETV-free mice at 5 DPI in **c**, showing GETV positive, indicating the GETV could be transmitted via an animal bite. Lanes 9 and 10, GETV-free mice in the right-hand cage in **e**, showing positive and negative at 5 DPI, demonstrating GETV transmitted from mice in the left-hand cage via mosquitos. Lanes 11-13, three mice in the right-hand cage in **f** tested negative, revealed that GETV is not an airborne virus. Tissue samples from the GETV-free (**i**) and GETV-infected mice (**j**) in a right-hand cage in experiment **e** were cultured in BHK21 cells, images were captured after 35 hours. Cells infected with GETV (**j**) obviously developed morphological characteristics, such as enlarged, rounded, refractile, pyknosis, and detachment cells.

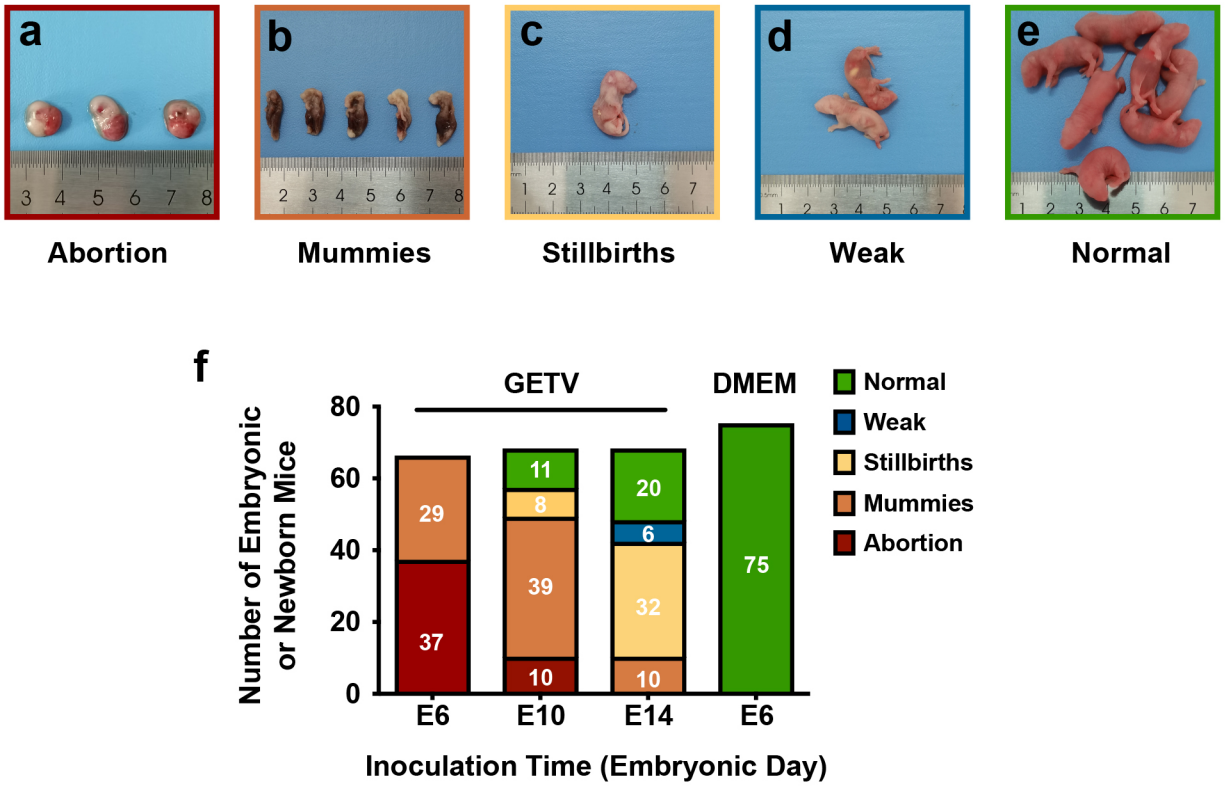


**Supplementary Figure S2. GETV caused reproductive disorders in pregnant mice.**

Twenty pregnant mice were randomly divided into four groups, and mice in the first three groups were inoculated oronasally with 100 μl ($10^6$ $TCID_{50}$/mL) GETV V1 strain at embryonic day 6 (E6, early-gestation), E10 (middle-gestation), and E14 (late-gestation), respectively. Mice in the fourth group were inoculated with an equal volume of DMEM at E6 as a control. Abortions (**a**, embryonic were expelled from the uterus before parturition), mummies (**b**, embryos were lost before farrowing), and stillbirths (**c**, embryos were lost around the time of birth, and might be prepartum or intrapartum) arising from GETV-infection were dominant in the E6, E10, and E14 groups. Some weak (**d**) and normal (**e**) newborns were found in E10 and E14 groups. **f**, Summary of the proportion of embryonic or newborn mice in the four groups. Numbers in the color frames in each column represented the number of mice that have each reproductive disorder.

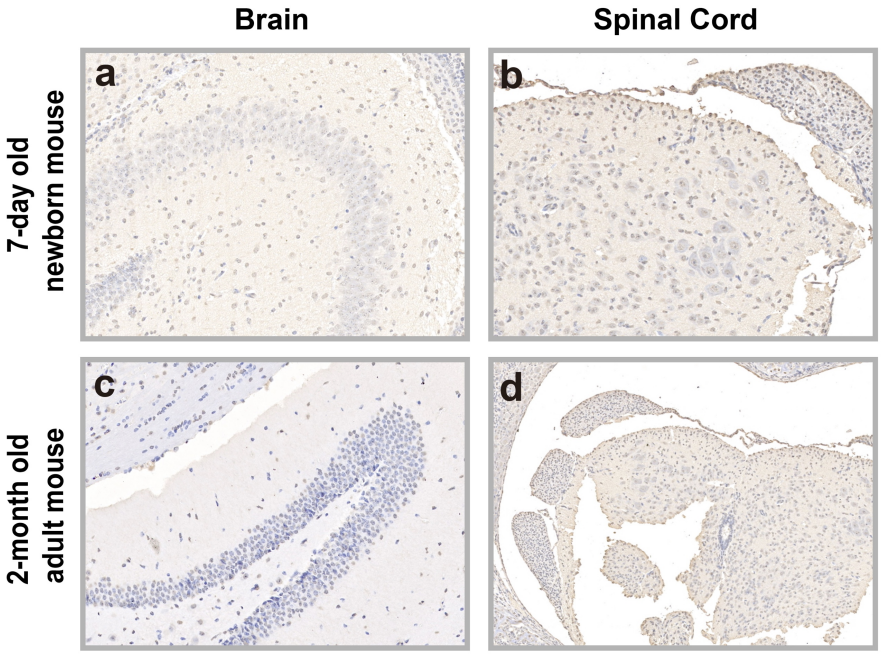


**Supplementary Figure S3. GETV antigen was not detected in the brain or spinal cord in 7-day-old newborn and 2-month-old adult mice that were inoculated with GETV.**

Forty 7-day-old newborn and forty 2-month-old adult mice were randomly divided into two groups, inoculated oronasally with 10 μl ($10^6$TCID$_{50}$/mL) GETV strain GETV-V1 or control DEME. Mice were held under clinical observation after inoculation. **a** and **b**, No GETV antigen was detected in the hippocampal dentate gyrus of the brain or spinal cord from 7-day-old mice 3 DPI. **c** and **d**, No GETV antigen was found in 2-month-old mice 3 DPI. Monoclonal antibody against capsid protein of GETV was used for immuno-histochemical assays.

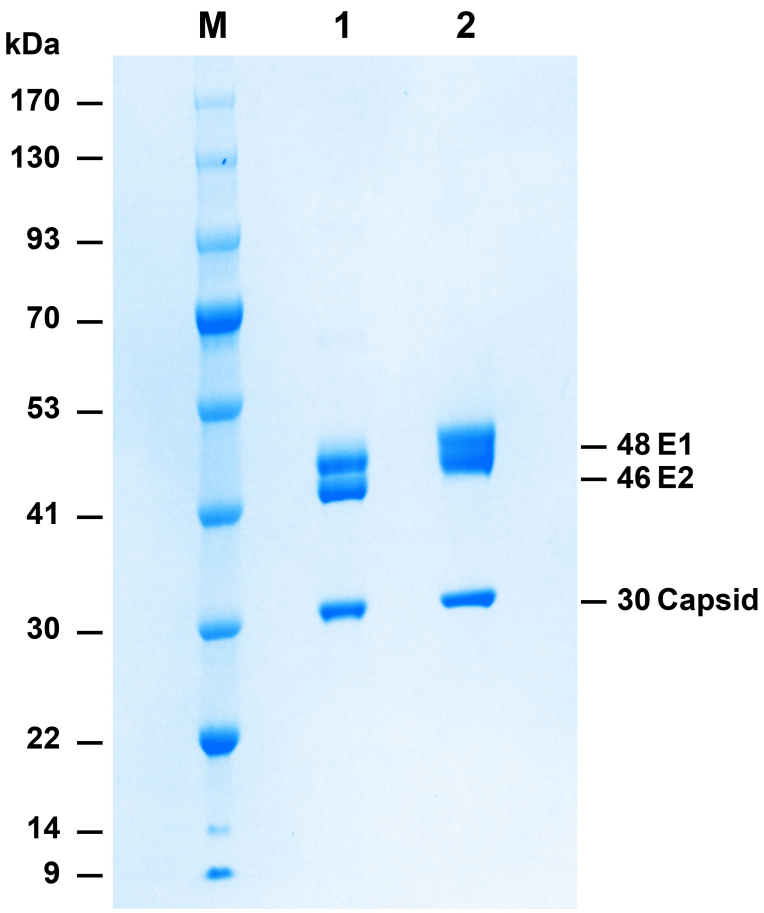


**Supplementary Figure S4. Protein contents of purified GETV were analyzed by polyacrylamide gel electrophoresis.**

Purified GETV samples were separated by 4-12% gradient SDS-PAGE (Bio-Rad) and the protein contents were stained with Coomassie brilliant blue. Three major structural proteins, E1, E2, and Capsid, are clearly identified. Lane M, protein markers; Lane 1, GETV proteins were separated under non-reducing conditions; Line 2, proteins were separated under reducing conditions.

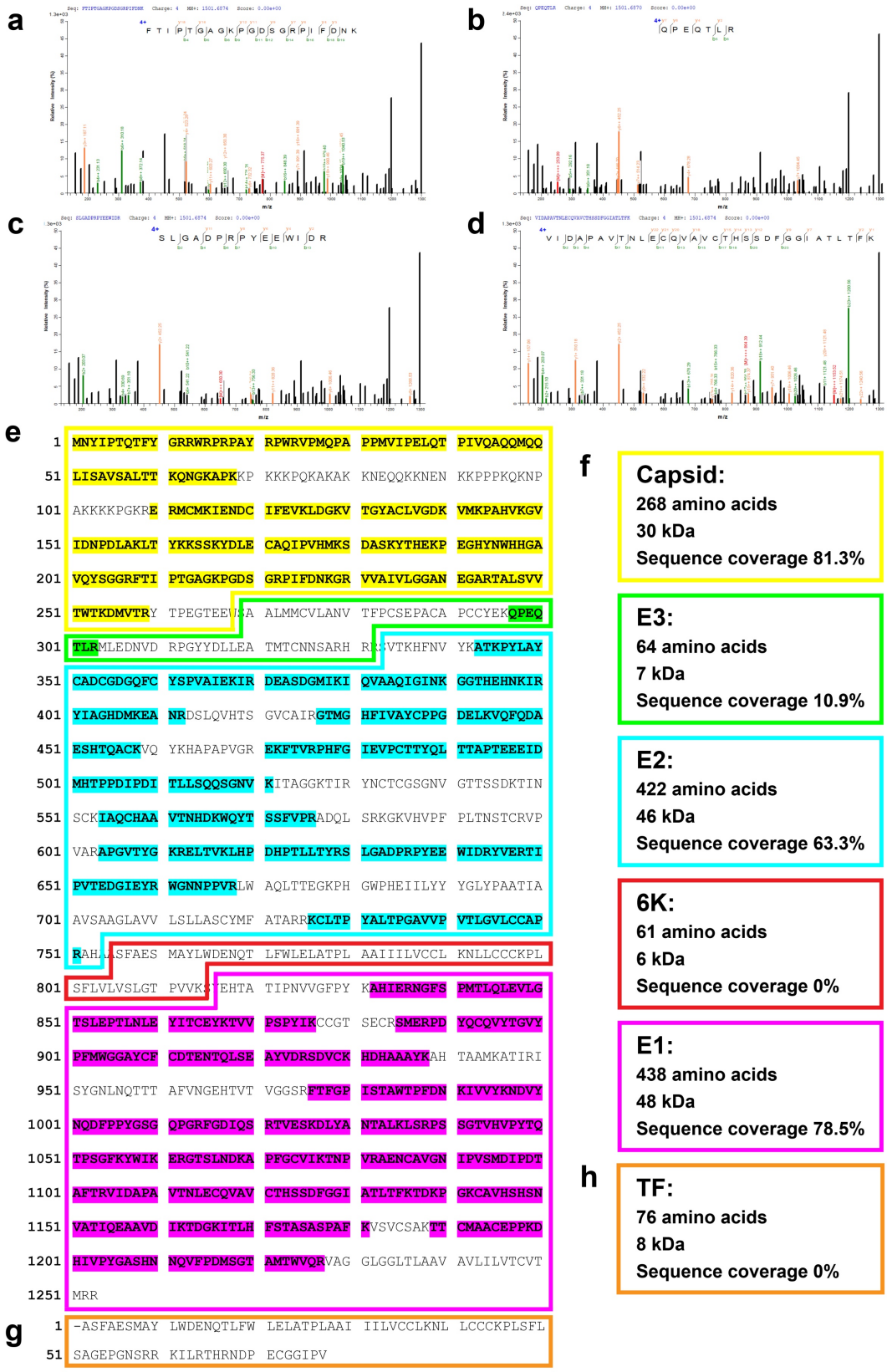


**Supplementary Figure S5. Mass spectrometry of GETV structural proteins.**

The protein contents of purified GETV samples were further analyzed with protein mass spectrometry. Representative peptide spectra from Capsid (**a**), E3 (**b**), E2 (**c**) and E1 (**d**). **e**, Four GETV-encoded structural proteins previously described were identified by mass spectrometry. **f,** Capsid, E1, and E2 that were highly abundant in SDS-PAGE analyses were displayed a higher score of sequence coverage, 81.3%, 78.5%, and 63.3%, respectively. Only one small peptide from the structural protein E3 was identified, and sequence coverage is 10.9%. Peptide from the structural protein 6K was not detected. **g**, The *6K* gene produced two distinct protein products, 6K and transframe (TF). This occurred via a (−1) ribosomal frameshift site that is highly conserved across the alphaviruses. The 6K and TF proteins each contain an identical N-terminal transmembrane domain (first 49 amino acids) and unique C-terminal ends[3]. **h**, Peptide from protein TF was not detected.

**a**

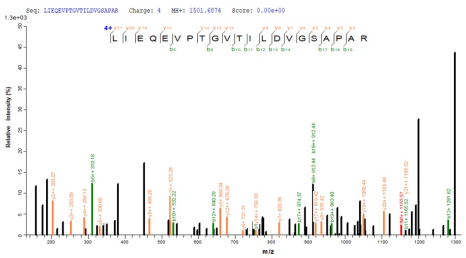

**b**

```
   1 MKVTVDVEAD SPFLKALQKA FPAFEVESQQ VTPNDHANAR AFSHLATKLI
  51 EQEVPTGVTI LDVGSAPARR LMSDHTYHCI CPMKSAEDPE RLANYARKLA
 101 KASGTVLDKN VSGKITDLQD VMATPDLESP TFCLHTDETC RTRAEVAVYQ
 151 DVYAVHAPTS LYHQAIKGVR TAYWIGFDTT PFMFEALAGA YPAYSTNWAD
 201 EQVLQARNIG LCATGLSEGR RGKLSIMRKK CLRPSDRVMF SVGSTLYTES
 251 RKLLRSWHLP SVFHLKGKNS FTCRCDTVVS CEGYVVKKIT ISPGIYGKTV
 301 DYAVTHHAEG FLMCKITDTV RGERVSFPVC TYVPATICDQ MTGILATDVT
 351 PEDAQKLLVG LNQRIVVNGR TQRNTNTMKN YLLPVVAQAF SKWAREARAD
 401 MEDEKPLGTR ERTLTCCCLW AFKSHKIHTM YKRPETQTIV KVPSTFDSFV
 451 IPSLWSSSLS MGIRQRIKLL LSARMAQGLP YSGDRTEARA AEEEEKEVQE
 501 AELTRAALPP LVSGSCADDI AQVDVEELTF RAGAGVVETP RNALKVTPQA
 551 HDHLIGSYLI LSPQTVLKSE KLAPIHPLAE QVTVMTHSGR SGRYPVDKYD
 601 GRVLIPTGAA IPVSEFQALS ESATMVYNER EFINRKLHHI ALYGPALNTD
 651 EESYEKVRAE RAETEYVFDV DKKACIKKEE ASGLVLTGDL INPPFHEFAY
 701 EGLKIRPAAP YHTTIIGVFG VPGSGKSAII KNMVTTRDLV ASGKKENCQE
 751 IMNDVKRQRG LDVTARTVDS ILLNGCKKGV ENLYVDEAFA CHSGTLLALI
 801 ALVRPSGKVV LCGDPKQCGF FNLMQLKVHY NHNICTRVLH KSISRRCTLP
 851 VTAIVSTLHY QGKMRTTNRC NTPIQIDTTG SSKPASGDIV LTCFRGWVKQ
 901 LQIDYRGHEV MTAAASQGLT RKGVYAVRQK VNENPLYSPL SEHVNVLLTR
 951 TENRLVWKTL SGDPWIKVLT NVPRGDFSAT LEEWHEEHDG IMRVLNERPA
1001 EVDPFQNKAK VCWAKCLVQV LETAGIRMTA DEWNTILAFR EDRAYSPEVA
1051 LNEICTRYYG VDLDSGLFSA QSVSLFYENN HWDNRPGGRM YGFNHEVARK
1101 YAARFPFLRG NMNSGLQLNV PERKLQPFSA ECNIVPSNRR LPHALVTSYQ
1151 QCRGERVEWL LKKIPGHQML LVSEYNLVIP HKRVFWIAPP RVSGADRTYD
1201 LDLGLPMDAG RYDLVFVNIH TEYRQHHYQQ CVDHSMRLQM LGGDSLHLLR
1251 PGGSLLMRAY GYADRVSEMV VTALARKFSA FRVLRPACVT SNTEVFLLFS
1301 NFDNGRRAVT LHQANQKLSS MYACNGLHTA GQAPSYRVRR ADISGHSEEA
1351 VVNAANAKGT VSDGVCRAVA KKWPSSFKGA ATPVGTAKMI RADGMTVIHA
1401 VGPNFSTVTE AEGDRELAAA YRAVASIIST NNIKSVAVPL LSTGTFSGGK
1451 DRVMQSLNHL FTALDATDAD VVIYCRDKNW EKKIQEAIDR RTAIELVSED
1501 VTLETDLVRV HPDSCLVGRN GYSATDGKLY SYLEGTRFHQ TAVDMAEIST
1551 LWPRLQDANE QICLYALGET MDSIRTKCPV EDADSSTPPK TVPCLCRYAM
1601 TAERVARLRM NNTKNIIVCS SFPLPKYRIE GVQKVKCDRV LIFDQTVPSL
1651 VSPRKYIQQP PEQLDNVSLT STTSTGSAWS FPSETTYETM EVVAEVHTEP
1701 PIPPPRRRRA AVAQLRQDLE VTEEIEPYVT QQAEIMVMER VATTDIRAIP
1751 VPARRAITMP VPAPRVRKVA TEPPLEPEAP IPAPRKRRTT STSPPHNPED
1801 FVPRVPVELP WEPEDLDIQF GDLEPRRRNT RDRDVSTGIQ FGDIDFNQSX
1851 LGRAQAYIFS SDTGPGHLQQ KSVRQHELPC ETLYAHEDER IYPPAFDGEK
1901 EKVLQAKMQM APTEANKSRY QSRKVENMKA LIVERLREGA KLYLHEQTDK
1951 VPTYTSKYPR PVYSPSVDDS LSDPEVAVAA CNSFLEENYP TVANYQITDE
2001 YDAYLDLVDG SESCLDRATF CPAKLRCYPK HHAYHQPQIR SAVPSPFQNT
2051 LQNVLAAATK RNCNVTQMRE LPTMDSAVFN VESFKKYACT GEYWQEFKDN
2101 PIRITTENIT TYVAKLKGPK AAALFAKTHN LVPLQEVPMD RFVMDMKRDV
2151 KVTPGTKHTE ERPKVQVIQA AEPLATAYLC GIHRELVRRL KAVLTPNIHT
2201 LFDMSAEDFD AIIAAHFQPG DAVLETDIAS FDKSQDDSLA LTALMLLEDL
2251 GVDQELLDLI EAAFGEITSV HLPTGTRFKF GAMMKSGMFL TLFINTLLNI
2301 VIACRVLRDK LSSSACAAFI GDDNIVHGVR SDPLMAERCA SWVNMEVKII
2351 DATMCEKPPY FCGGFILYDS VAGTACRVAD PLKRLFKLGK PLPADDNQDE
2401 DRRRALKDET VKWSRIGLRE ELDVALSSRY QVSGVGNITR AMSTLSKSLK
2451 SFRKIRGPII HLYGGPK
```

**c**

**nsP1:**
**534 amino acids**
**59 kDa**
**Sequence coverage 7.9%**

**nsP2:**
**798 amino acids**
**90 kDa**
**Sequence coverage 0%**

**nsP3:**
**523 amino acids**
**58 kDa**
**Sequence coverage 0%**

**nsP4:**
**612 amino acids**
**69 kDa**
**Sequence coverage 0%**

**Supplementary Figure S6. Mass spectrometry of GETV non-structural proteins.**

**a**, Representative peptide spectrum of non-structural-protein 1 (nsP1). **b** and **c**, Only three peptides were identified in nsP1, and sequence coverage for nsP1 is 7.9%. Peptides from nsP2, nsP3 or nsP4 were not detected.

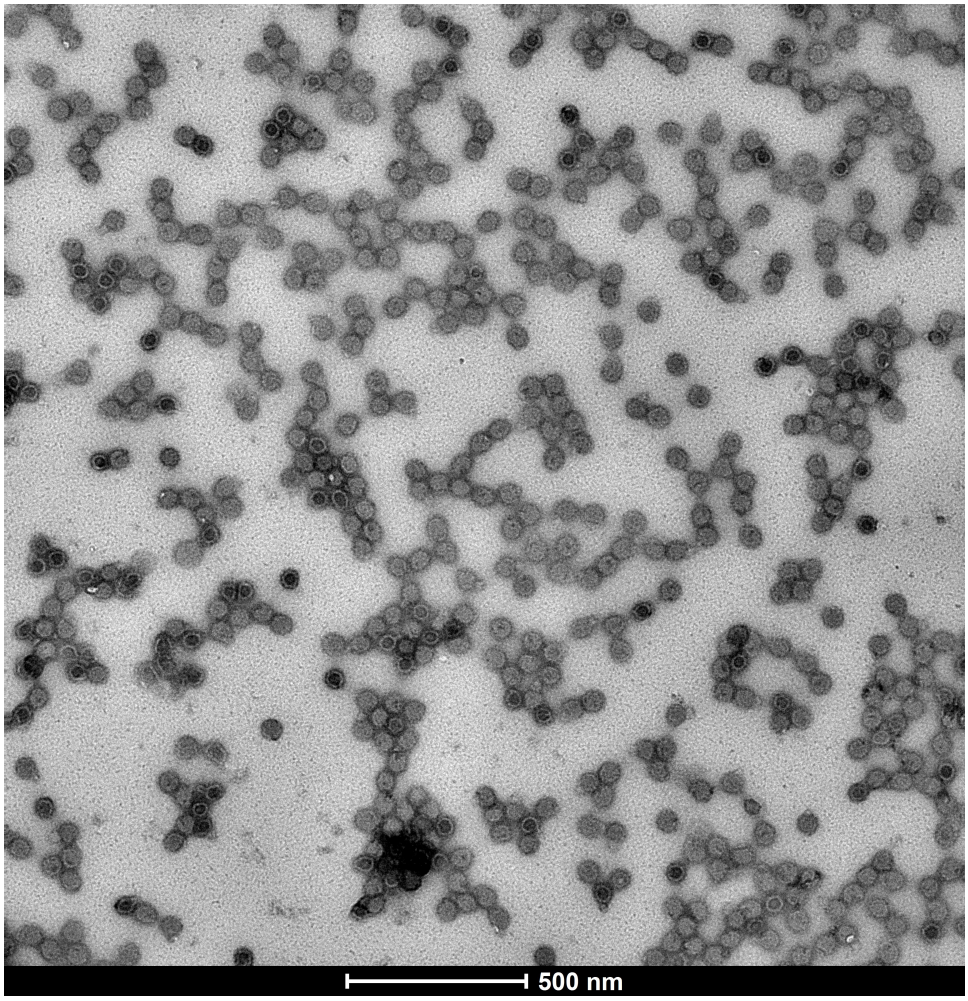


**Supplementary Figure S7. Negatively stained electron micrograph of GETV-V1 strain virions.**

Sucrose gradient purified GETV were negatively stained and imaged at 17,500X magnification.

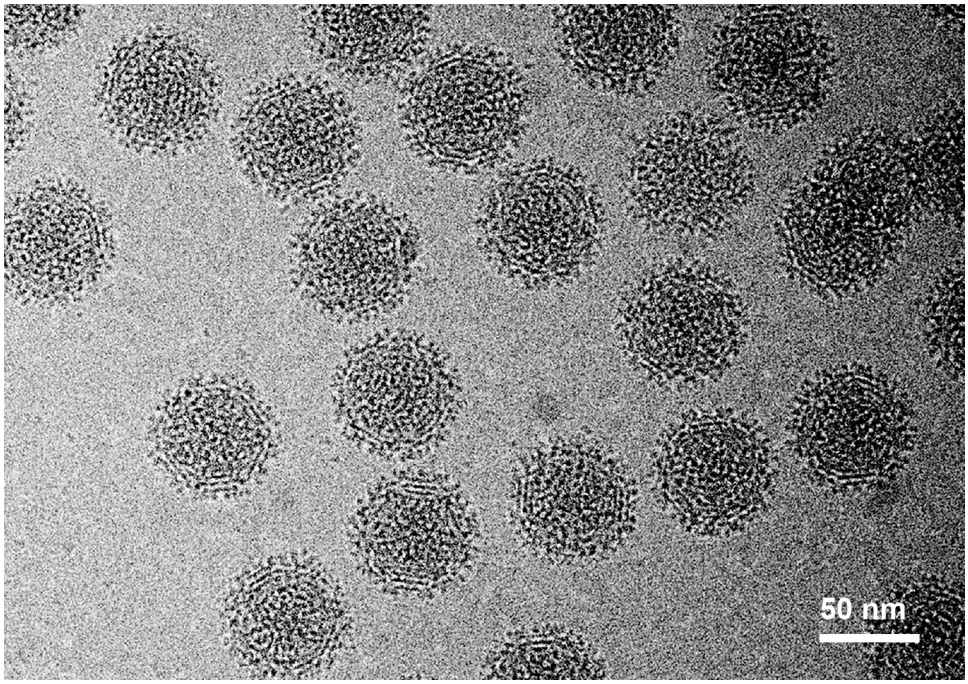


**Supplementary Figure S8. Cryo-electron micrograph of purified GETV virions.**

Micrographs were captured in a Thermo Fisher Scientific Titan Krios Cryo-Transmission Electron Microscope equipped with a Gatan K3 direct electron detector camera. Beam-induced shifting that blurred the captured images were corrected using MotionCor2[4].

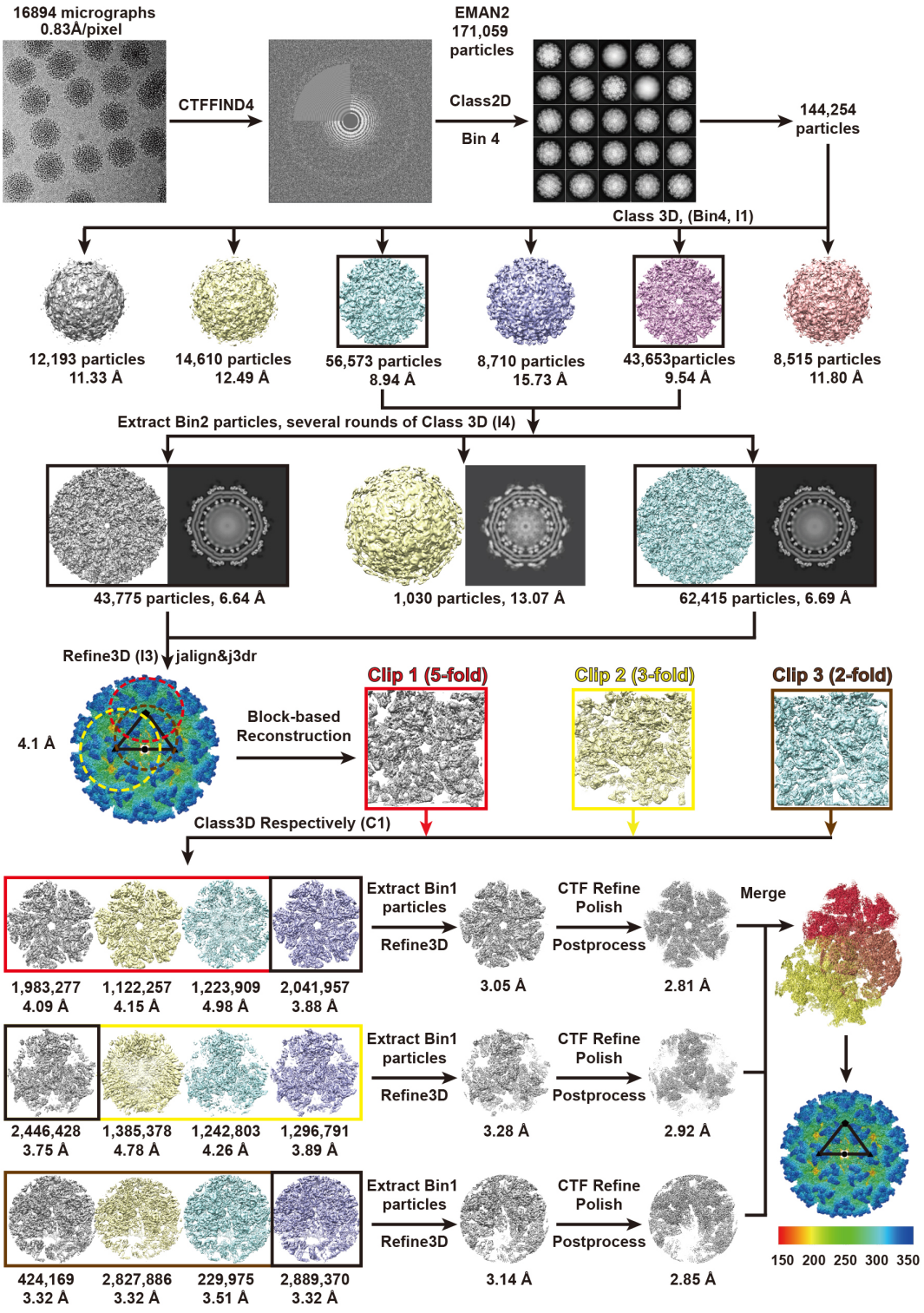


**Supplementary Figure S9. Cryo-EM image-processing workflow.**

Schematic of pre-processing, 2D and 3D classification, block-based reconstruction, and refinement procedures used to generate the 2.8-Å resolution density map.

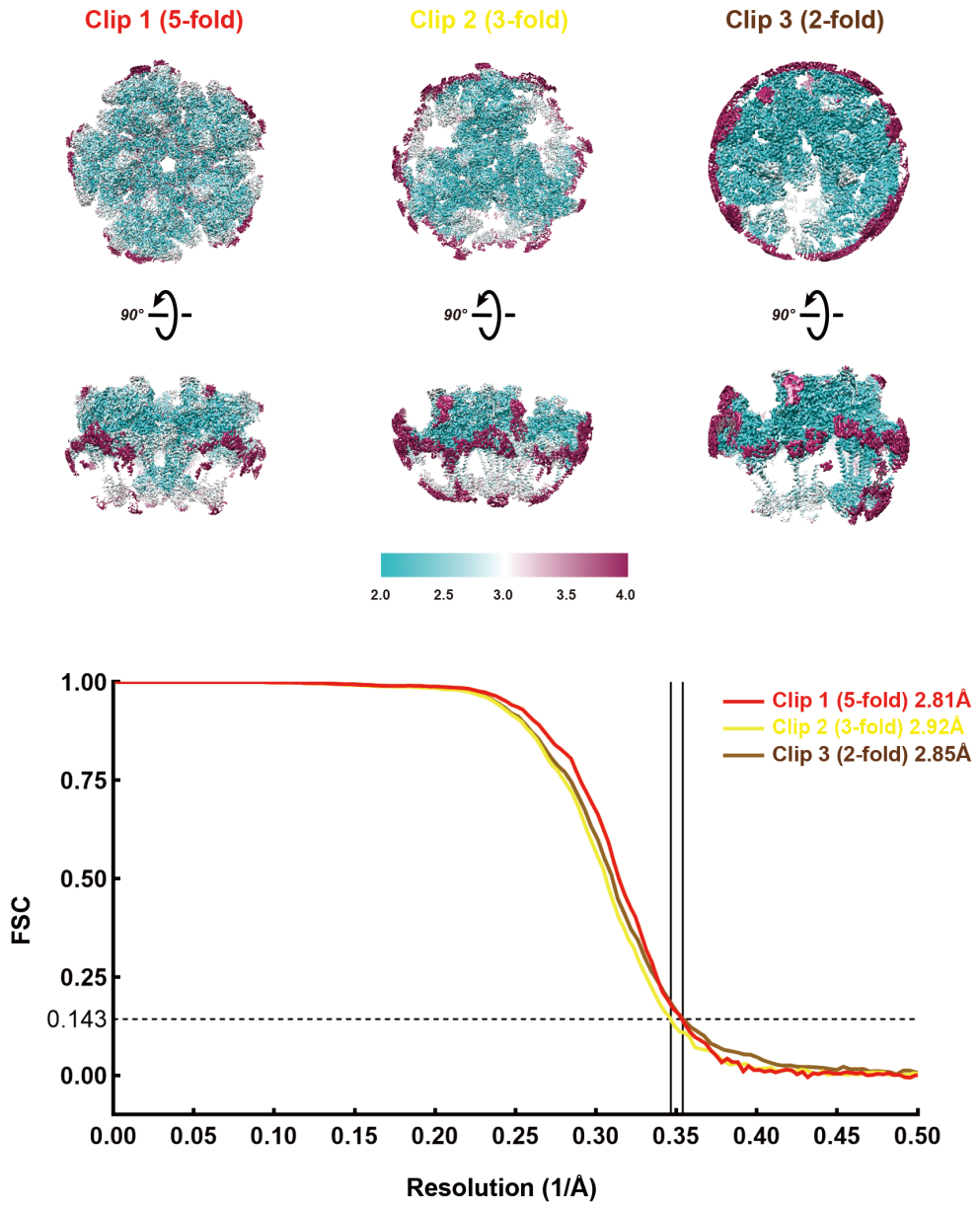


**Supplementary Figure S10. Local resolution of cryo-EM block-based reconstructions of GETV.**

Block-based reconstructions of GETV, colored according to local resolution. The resolution varies from 2.0 Å (sky blue) through 3.0 Å (light grey) to 4.0 Å (violet-red). Fourier shell correlation (FSC) curve of the final reconstructions indicating an average resolution of 2.81 Å, 2.92 Å, and 2.84 Å for the Clip 1 (5-fold symmetry), Clip 2 (3-fold), and Clip 3 (2-fold), respectively, according to the gold-standard criterion (FSC=0.143).

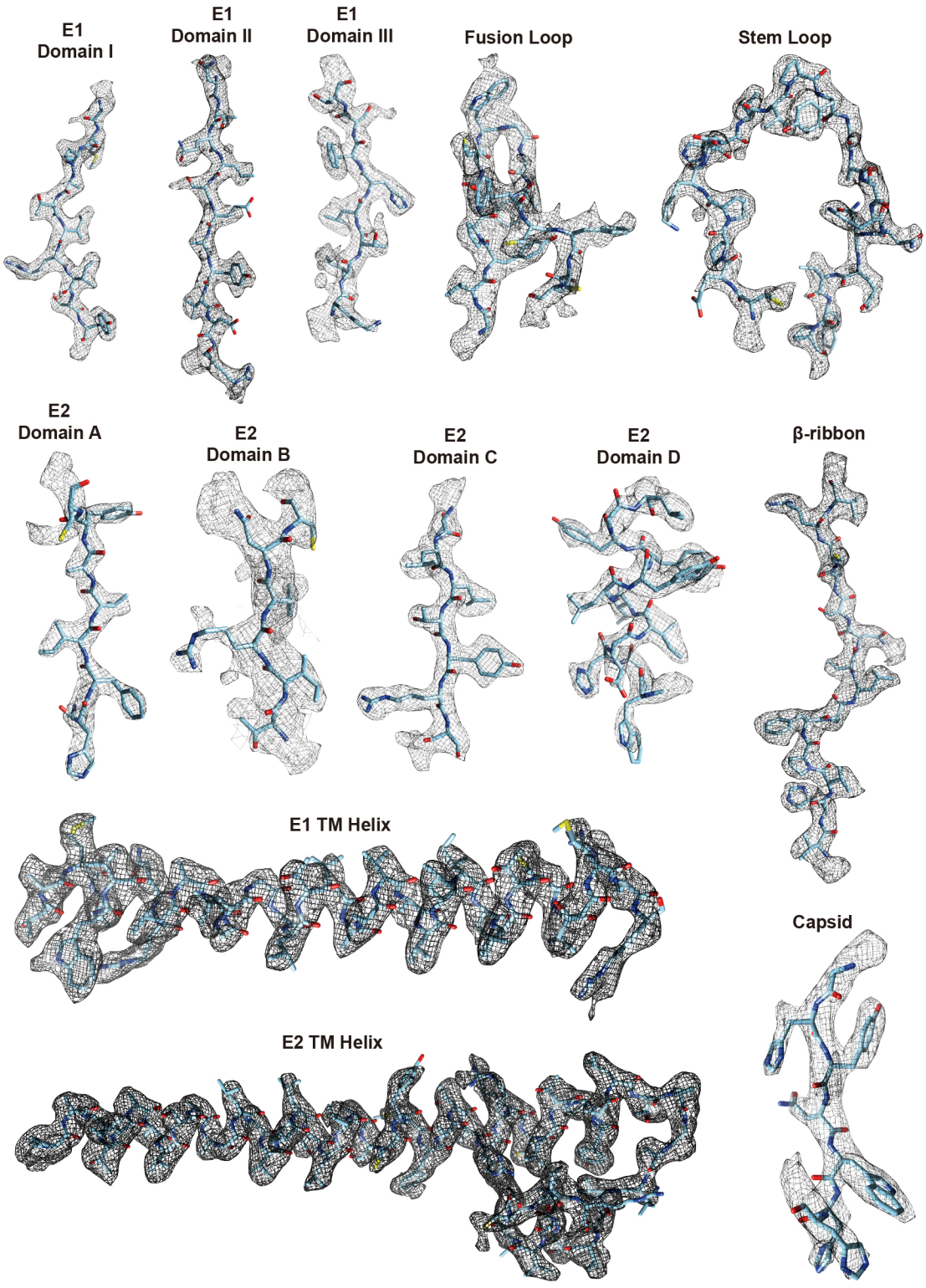


**Supplementary Figure S11. Representative density and atomic models of each domain of E1-E2-capsid heterotrimer.**

E1 Domain I, residues A128-Y137; E1 Domain II, residues N100-R110; E1domainIII, residues K351-T358; Fusion loop, residues V84-T98, Stem-loop, residues C380-D401; E1 TM Helix, residues T405-R438; E2 Domain A, residues A92-H99; E2 Domain B, residues T196-C201; E2 Domain C, residues T292-S298; E2 Domain D, residues W350-L361; E2 β-ribbon, K253-V267; E2 TM Helix, residues Y362-R419; Capsid, residues E191-H198.

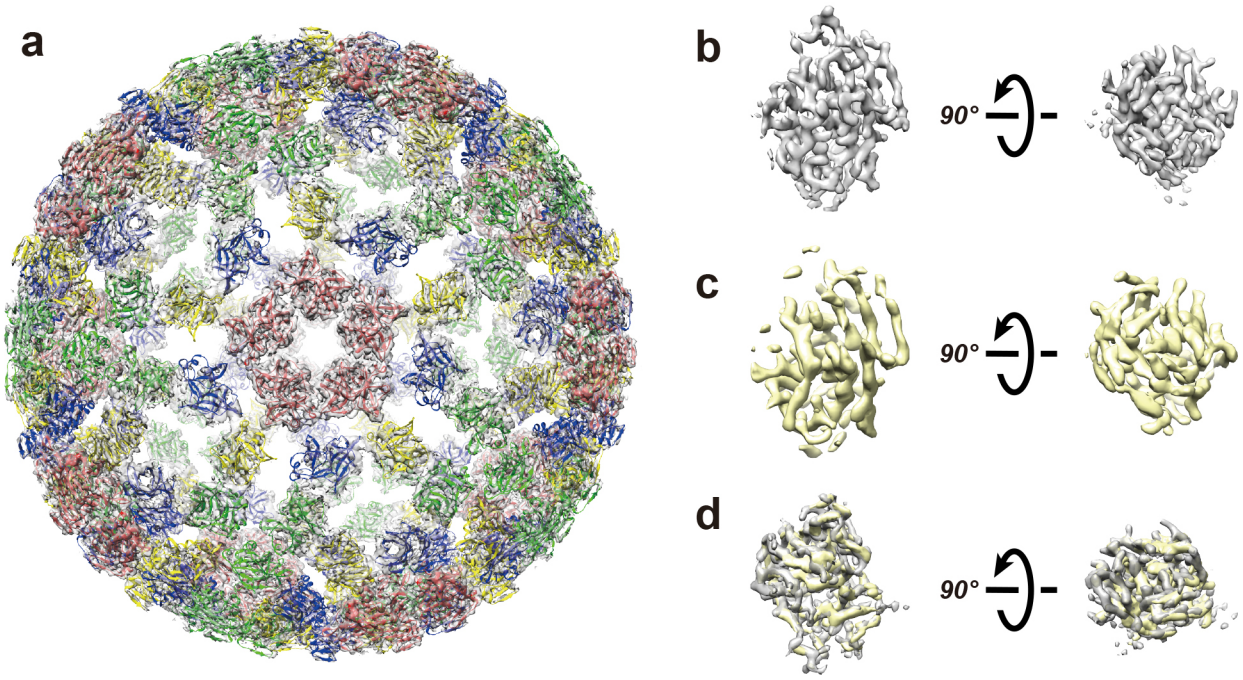


**Supplementary Figure S12. Density maps of the capsid.**

**a**, Density map of icosahedral capsid and atomic models. The pentamer capsids models are colored by red, and the other three hexamer capsids models are colored by green, yellow and blue separately. **b**, Density map of the pentamer capsid, **c**, Hexamer capsid, and **d**, Superpose map of pentamer capsid and hexamer capsid. The correlation value is 0.92.

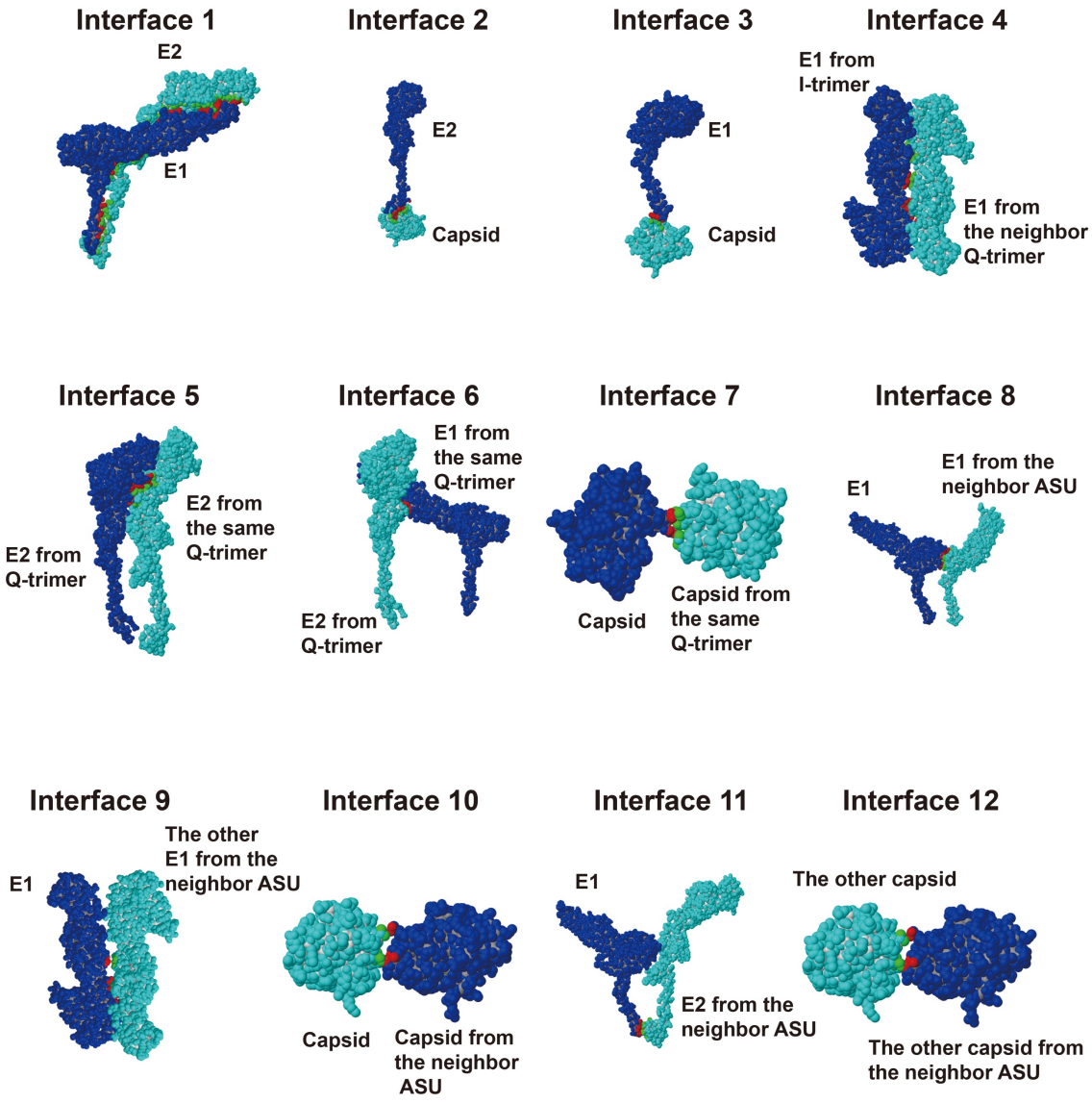


**Supplementary Figure S13. Interacting regions between GETV structural proteins.**

The interface areas were analyzed by using the PDBePISA server (https://www.ebi.ac.uk/pdbe/prot_int/pistart.html). The structures were rendered as space-fill. The interaction areas are colored in red or green. The relevant protein domains are colored in blue or cyan and labeled on the side. Interface areas, the number of hydrogen bonds ($N_{HB}$) and salt-bridges ($N_{SB}$) are listed in Supplementary Table S2.

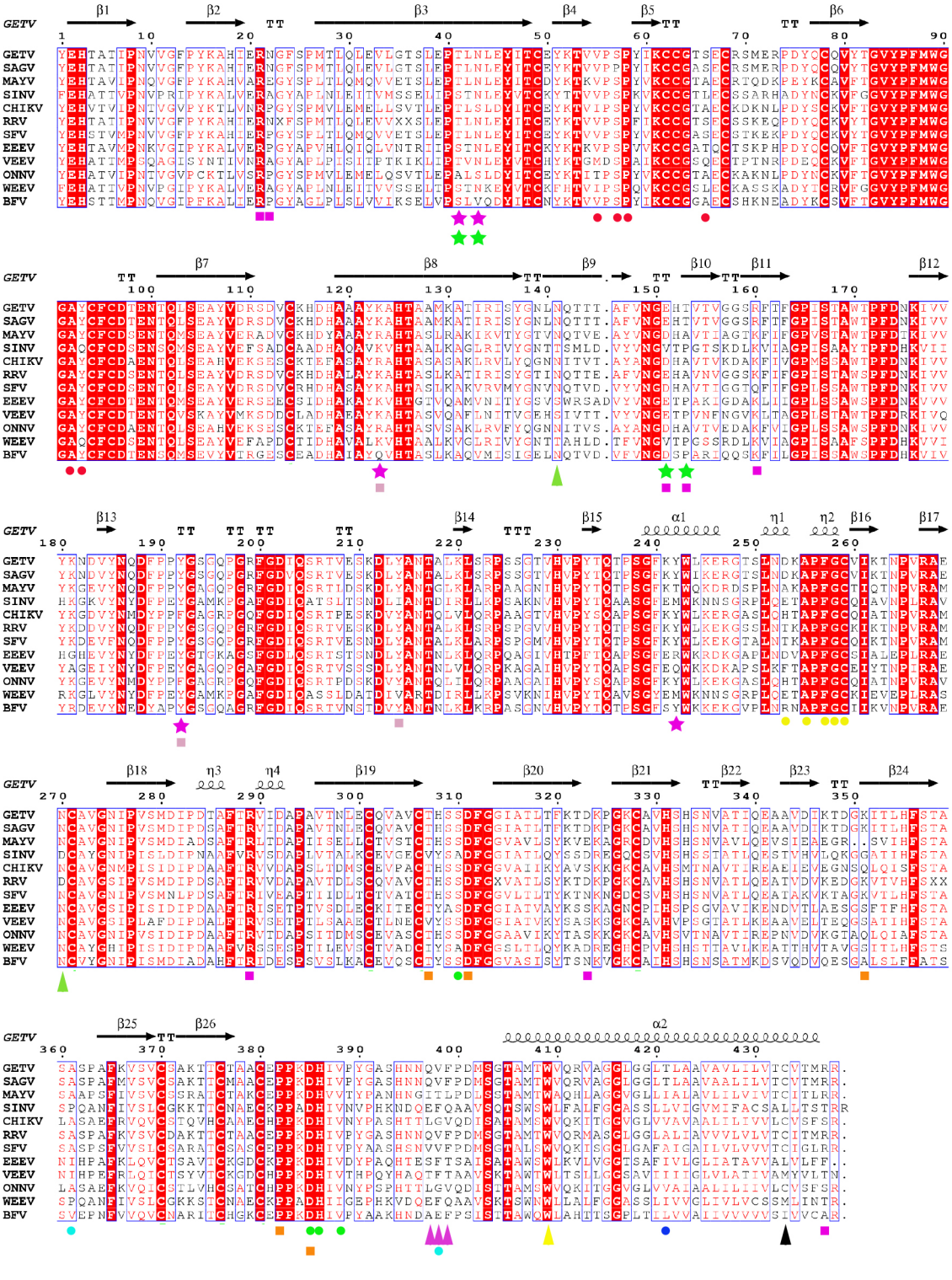


**Supplementary Figure S14. Multiple sequence alignment and secondary structural elements of alphaviruses E1 protein.**

Sequence alignment of E1 proteins from representative members of alphaviruses. The secondary structure elements are displayed above the sequences. Fully conserved residues and similar residues are shaded and shown in red. Sequences of structural polyprotein are from GETV (Getah virus, this study, ASA40294.1), SAGV (Sagiyama virus, BAA92847.1), MAYV (Mayaro virus, AZM66144.1), SINV (Sindbis virus, AYM45056.1), CHIKV (Chikungunya virus, NP_690589.2), RRV (Ross River virus, NP_062880.1), SFV (Semliki Forest virus, NP_463458.1), EEEV (Eastern equine encephalitis virus, NP_632022.1), VEEV (Venezuelan equine encephalitis virus, NP_040824.1), ONNV (O'nyong nyong virus, NP_041255.1), WEEV (Western equine encephalitis virus, NP_640331.1), and BFV (Barmah Forest virus, NP_054024.1). N-glycosylation sites and S-acylation sites are marked by green and black triangles. Magenta and yellow triangles represent residues that interact with cholesterol and DOPC respectively. The colored dots represent residues that interact between E1 and E2, or E2 and capsid. Dots' colors are the same as the borders of Figure 2b-2e. The colored stars represent residues that interact within the ASU. Stars' colors are the same as the corresponding residues of Figure 3b-3f. The colored squares represent residues that interact between two Q-trimers. Squares' colors are the same as the corresponding residues of Figure 4b-4g.

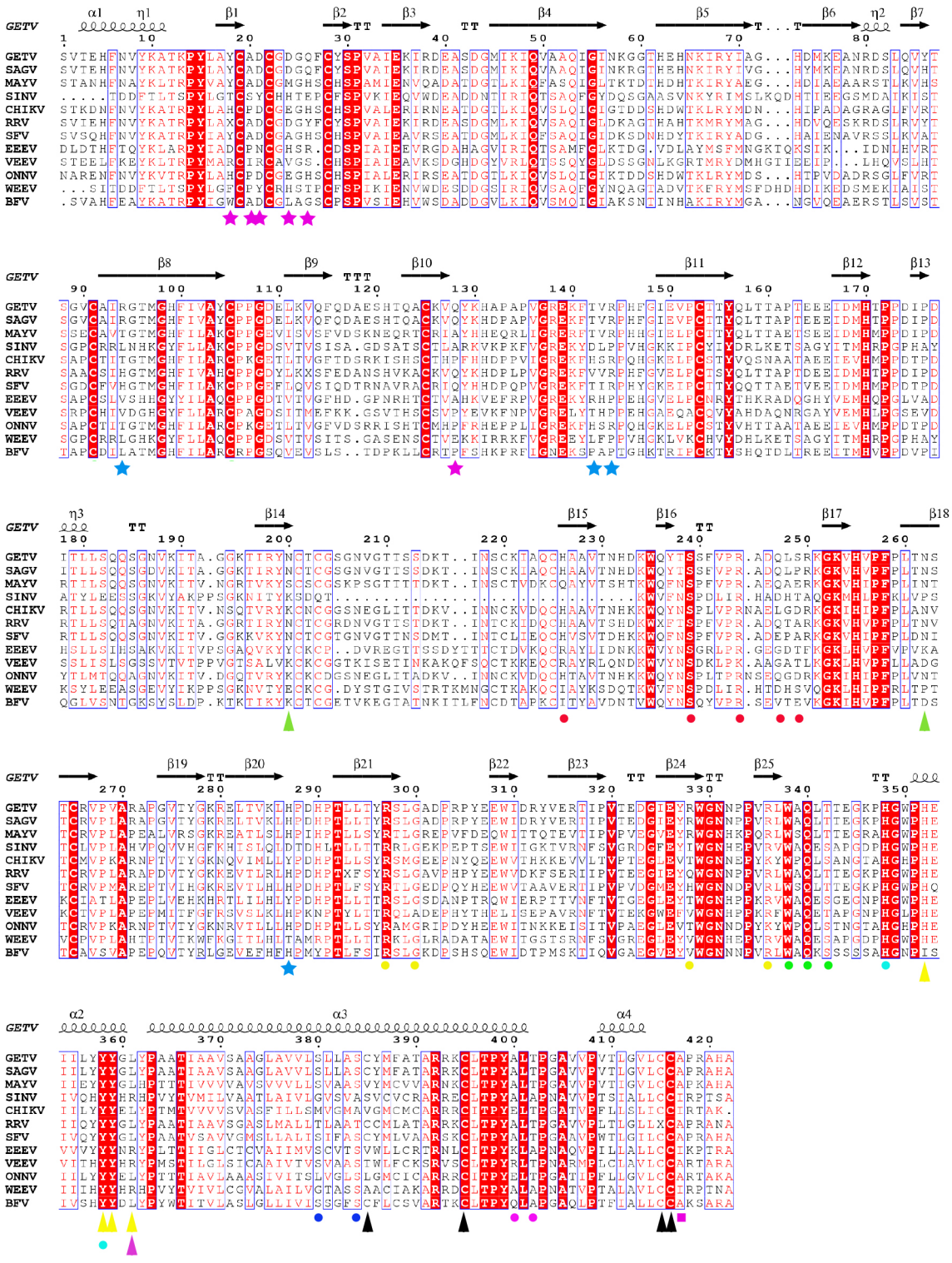


**Supplementary Figure S15. Multiple sequences alignment and secondary structural elements of alphaviruses E2 protein.**

Sequence alignment of the E2 proteins from representative members of alphaviruses. The secondary structure elements are displayed above the sequences. Fully conserved residues and similar residues are shaded and shown in red. Structural polyprotein sequences and the markers for key residues are the same as in Supplementary Figure S14.

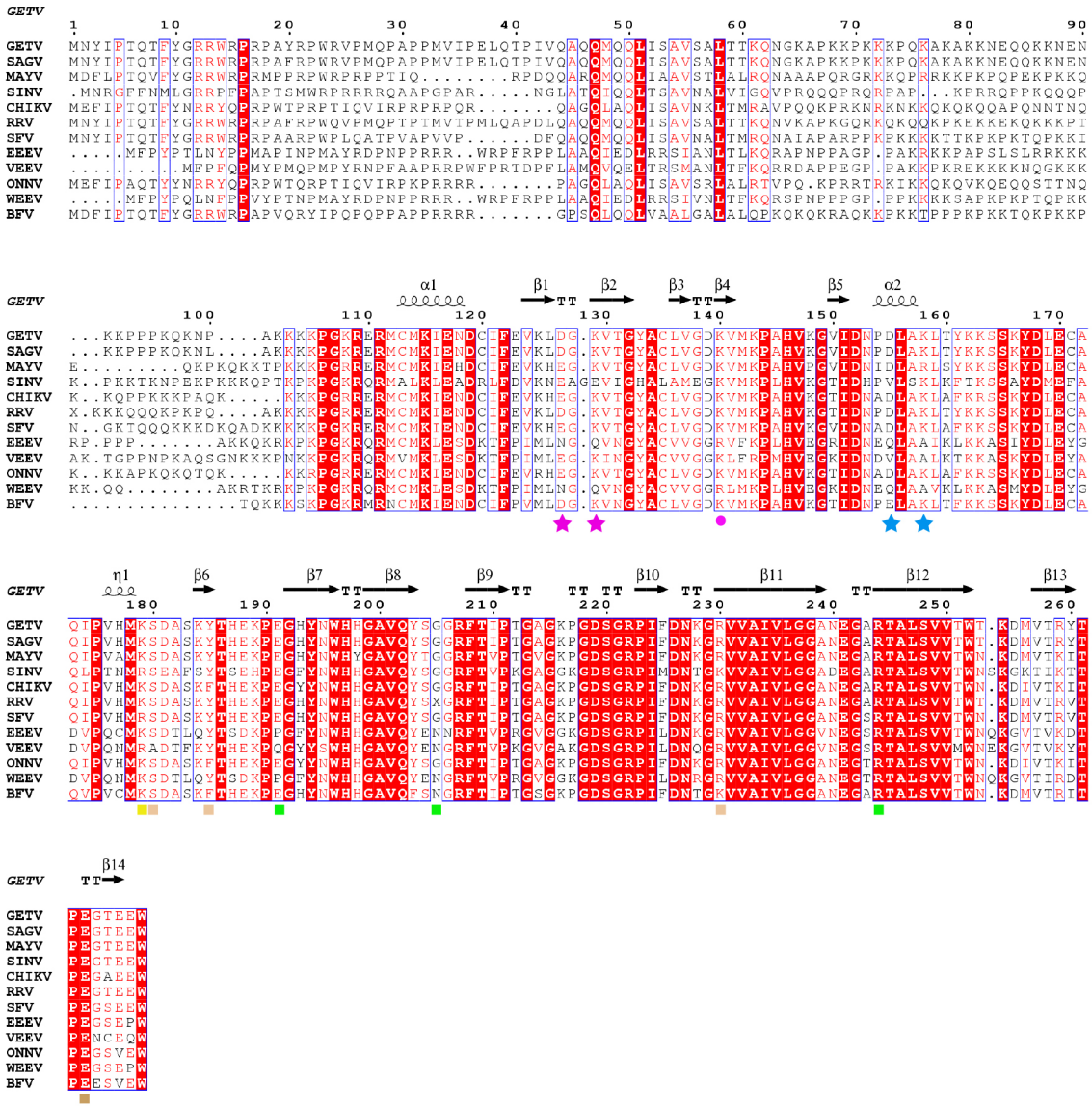


**Supplementary Figure S16. Multiple sequences alignment and secondary structural elements of alphaviruses capsid protein.**

Sequence alignment of capsid proteins from representative members of alphaviruses. The secondary structure elements are displayed above the sequences. Fully conserved residues and similar residues are shaded and shown in red. Structural polyprotein sequences and the markers for key residues are the same as in Supplementary Figure S14.

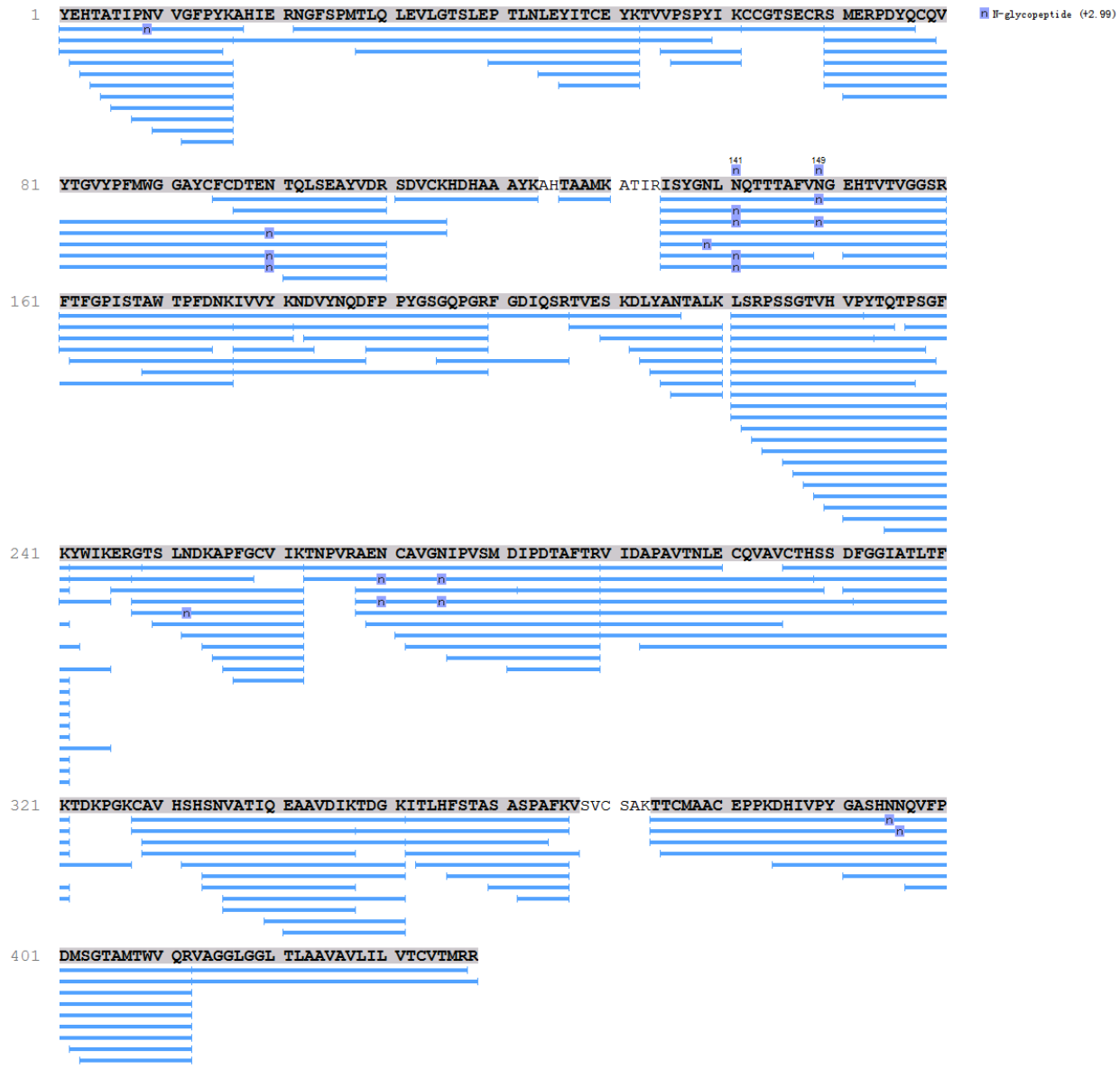


**Supplementary Figure S17. Mass spectrometry of the N-glycosylation sites in the GETV E1 protein.**

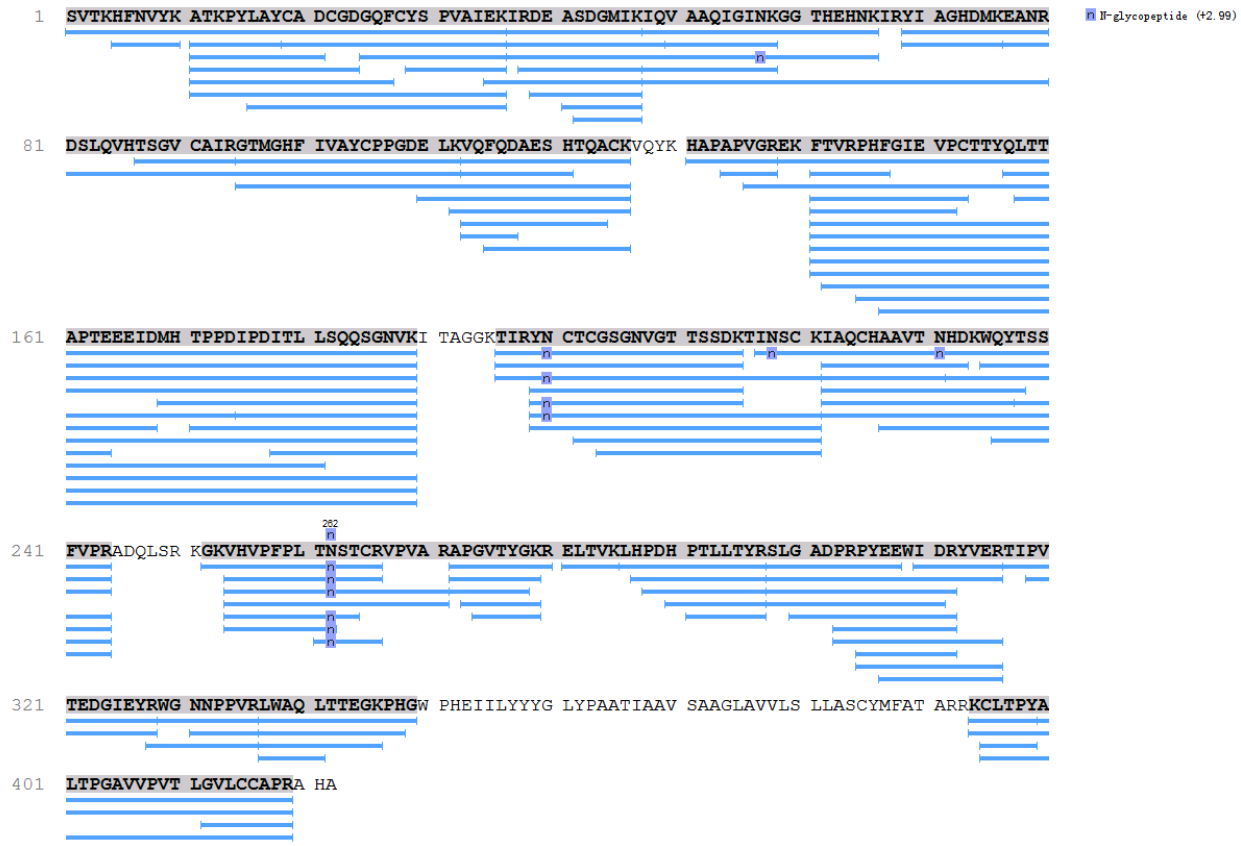


**Supplementary Figure S18. Mass spectrometry of the N-glycosylation sites in the GETV E2 protein.**

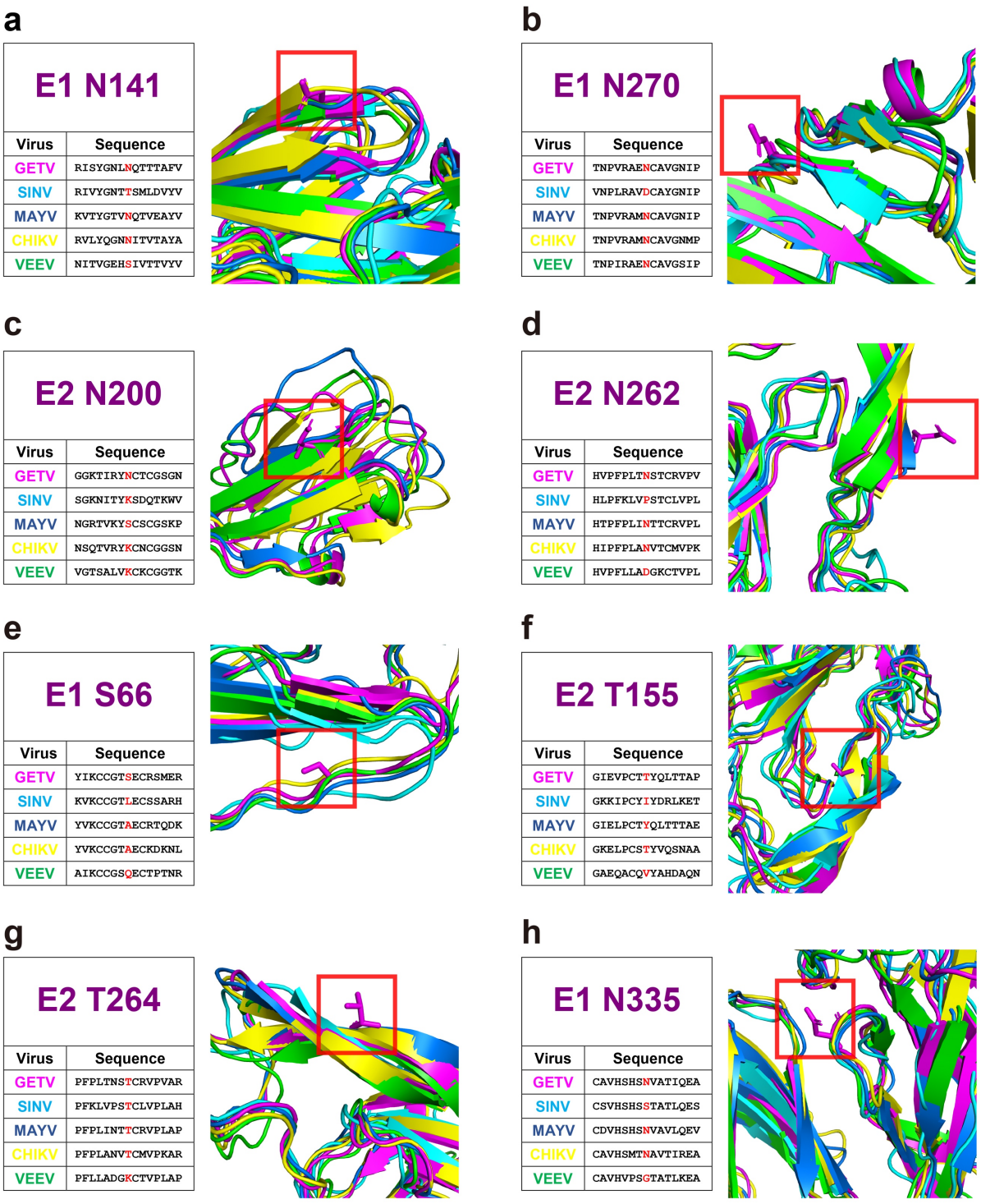


**Supplementary Figure S19. Conserved glycosylation sites in alphaviruses.**

**a-h,** Structural differences among alphaviruses at the eight glycosylation sites. Tables on the left show amino acid sequences around the sites, with glycosylation residues

highlighted in red. Figures on the right display the five atomic structures of alphaviruses aligned to the GETV atomic model. The GETV model is colored in magenta, the SINV model in cyan (PDB ID: 6IMM), the MAYV model in marine (PDB ID: 7KO8), the CHIKV model in yellow (PDB ID: 6NK5), and the VEEV model in green (PDB ID: 3J0C).

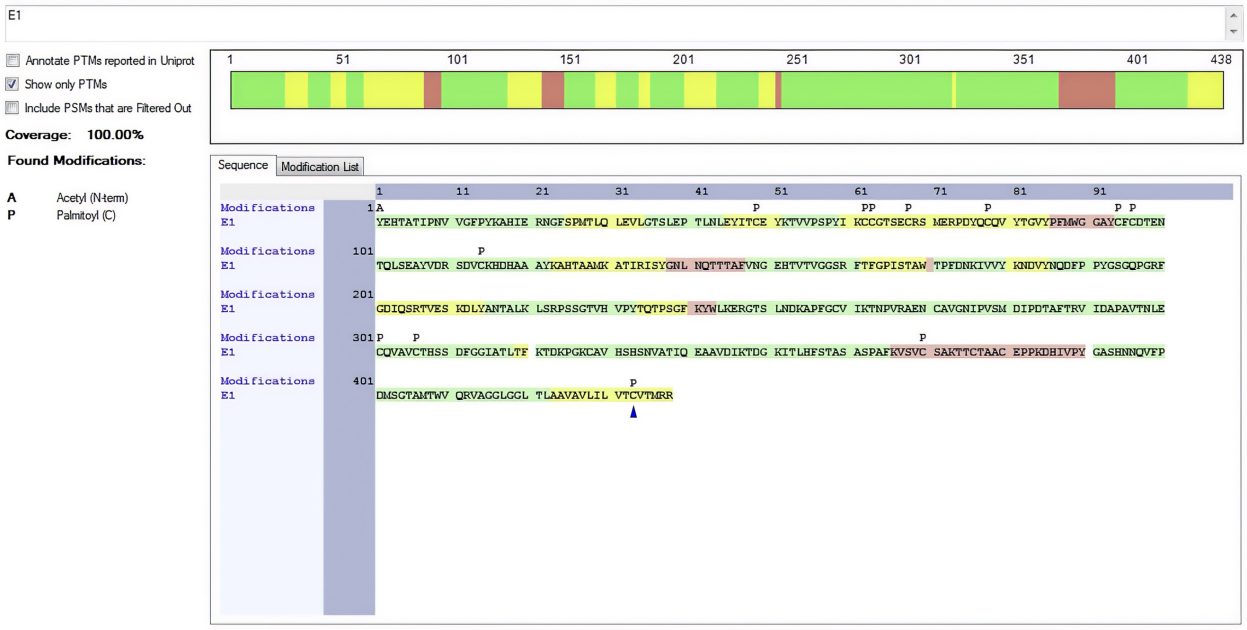


**Supplementary Figure S20. Mass spectrometry of the S-acylation sites in the GETV E1 protein.**

The protein sequence coverage bar graphically represents the protein sequence. The colored areas represent portions of the protein sequence that match peptides. The protein sequence coverage bar is colored to indicate the confidence of the peptide sequence identification: green, high-confidence peptides; yellow, medium-confidence peptides; pink, low-confidence peptides. Single-letter abbreviation “P” above the sequence indicates the identified palmitoyl sites by mass spectrometry, and the blue arrowhead points to the position of the C433 palmitoylation site identified in the cryo-EM density map.

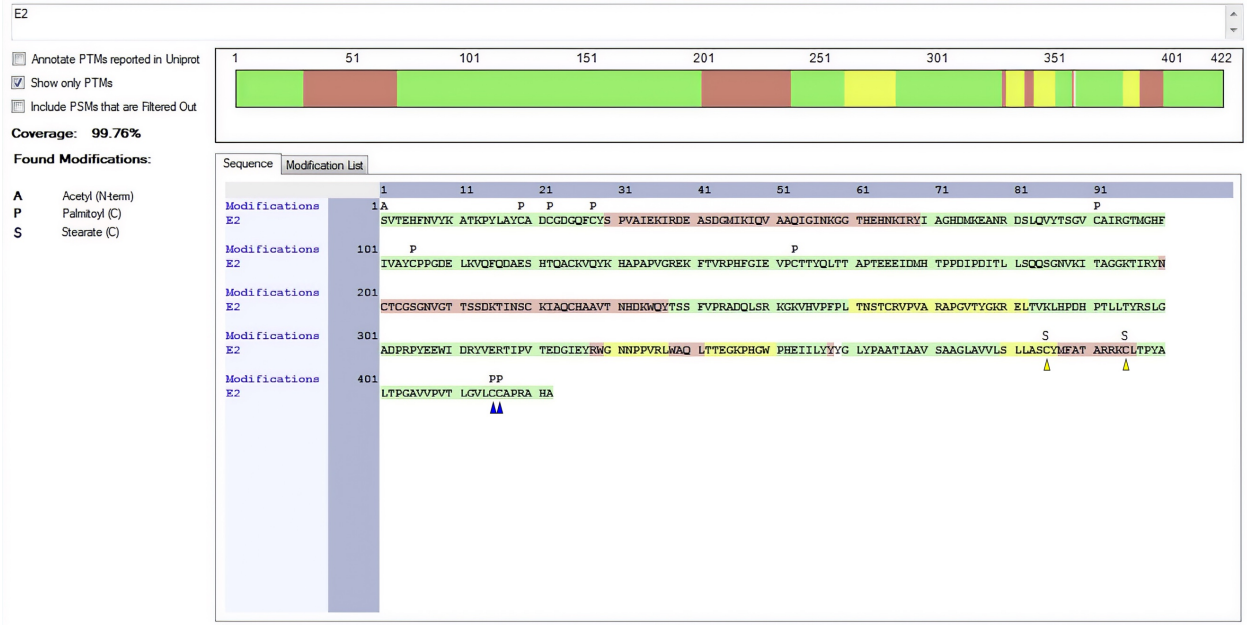


**Supplementary Figure S21. Mass spectrometry of the S-acylation sites in the GETV E2 protein.**

Single-letters abbreviation “P” and “S” above the sequence indicate the identified palmitoyl or stearate sites by mass spectrometry, and blue and yellow arrowheads point to the positions of C385 and C395 stearate-acylation sites and C415 and C416 palmitoylation sites identified in the cryo-EM density map.

## E2 C385

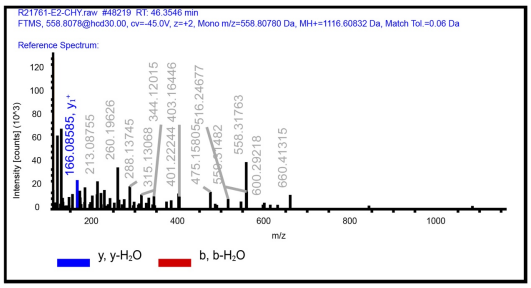


| #1 | b+ | b2+ | Seq. | y+ | y2+ | #2 |
|---|---|---|---|---|---|---|
| 1 | 114.09134 | 57.54931 | L | | | 7 |
| 2 | 185.12845 | 93.06787 | A | 1003.52426 | 502.26577 | 6 |
| 3 | 272.16048 | 136.58388 | S | 932.48715 | 466.74721 | 5 |
| 4 | 641.43062 | 321.21895 | C-Stearate | 845.45512 | 423.2312 | 4 |
| 5 | 804.49395 | 402.75061 | Y | 476.18498 | 238.59613 | 3 |
| 6 | 951.52935 | 476.26831 | M-Oxidation | 313.12165 | 157.06447 | 2 |
| 7 | | | F | 166.08626 | 83.54677 | 1 |

## E2 C395

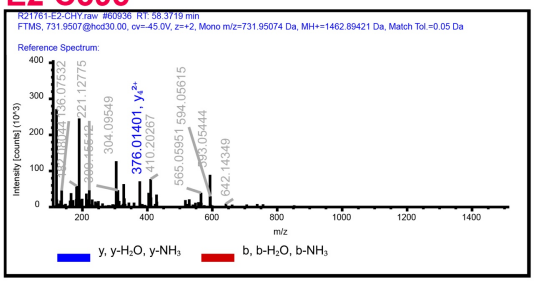


| #1 | b+ | b2+ | Seq. | y+ | y2+ | #2 |
|---|---|---|---|---|---|---|
| 1 | 132.04776 | 66.52752 | M | | | 10 |
| 2 | 279.11618 | 140.06173 | F | 1331.85955 | 666.43341 | 9 |
| 3 | 350.15329 | 175.58028 | A | 1184.79113 | 592.8992 | 8 |
| 4 | 451.20097 | 226.10412 | T | 1113.75402 | 557.38065 | 7 |
| 5 | 522.23808 | 261.62268 | A | 1012.70634 | 506.85681 | 6 |
| 6 | 678.33919 | 339.67323 | R | 941.66923 | 471.33825 | 5 |
| 7 | 834.4403 | 417.72379 | R | 785.56811 | 376.01401 | 4 |
| 8 | 962.53527 | 481.77127 | K | 629.467 | 315.23714 | 3 |
| 9 | 1331.8054 | 666.40634 | C-Stearate | 501.37204 | 251.18966 | 2 |
| 10 | | | L | 132.10191 | 66.55459 | 1 |

## E2 C415  E2 C416

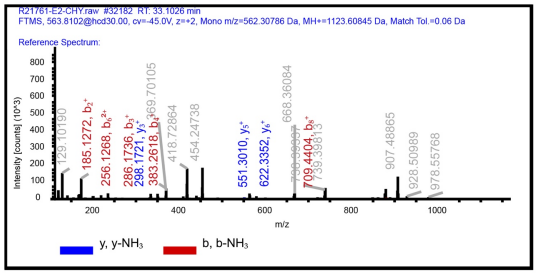


| #1 | b+ | b2+ | Seq. | y+ | y2+ | #2 |
|---|---|---|---|---|---|---|
| 1 | 72.0449 | 36.5225 | A | | | 23 |
| 2 | 185.1272 | 93.0645 | L | 2621.6265 | 1311.3132 | 22 |
| 3 | 286.1736 | 143.5883 | T | 2508.5422 | 1254.7711 | 21 |
| 4 | 383.2618 | 192.1147 | P | 2407.4946 | 1204.2473 | 20 |
| 5 | 440.2509 | 220.6254 | G | 2310.4419 | 1155.7209 | 19 |
| 6 | 511.288 | 256.1268 | A | 2253.4204 | 1127.2102 | 18 |
| 7 | 610.3564 | 305.6782 | V | 2182.3833 | 1091.6917 | 17 |
| 8 | 709.4404 | 355.2124 | V | 2083.3149 | 1042.1575 | 16 |
| 9 | 806.4776 | 403.7388 | P | 1984.2285 | 992.6024 | 15 |
| 10 | 905.546 | 453.273 | V | 1887.1937 | 944.0969 | 14 |
| 11 | 1006.5937 | 503.7968 | T | 1788.1099 | 894.5627 | 13 |
| 12 | 1119.6777 | 560.3389 | L | 1687.0723 | 844.0388 | 12 |
| 13 | 1176.6992 | 588.8496 | G | 1573.9812 | 787.4968 | 11 |
| 14 | 1275.7676 | 638.3838 | V | 1516.9534 | 758.9861 | 10 |
| 15 | 1388.8517 | 694.9258 | L | 1417.8982 | 709.4404 | 9 |
| 16 | 1730.0906 | 865.5453 | C-Plamitoyol | 1304.8132 | 652.9099 | 8 |
| 17 | 2071.3293 | 1036.1647 | C-Plamitoyol | 963.5817 | 482.2904 | 7 |
| 18 | 2142.3665 | 1071.6832 | A | 622.3352 | 311.671 | 6 |
| 19 | 2239.4192 | 1120.2096 | P | 551.301 | 276.1524 | 5 |
| 20 | 2395.5203 | 1198.2601 | R | 454.2521 | 227.626 | 4 |
| 21 | 2466.5574 | 1233.7787 | A | 298.1721 | 149.5755 | 3 |
| 22 | 2603.6165 | 1302.3082 | H | 227.1139 | 114.0569 | 2 |
| 23 | | | A | 90.0549 | 45.5275 | 1 |

## E1 C433

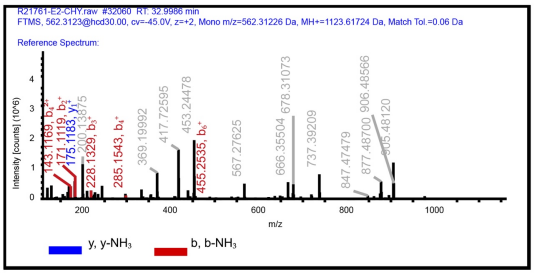


| #1 | b+ | b2+ | Seq. | y+ | y2+ | #2 |
|---|---|---|---|---|---|---|
| 1 | 100.0762 | 50.5381 | V | | | 26 |
| 2 | 171.1119 | 86.0567 | A | 2709.6497 | 1355.3248 | 25 |
| 3 | 228.1329 | 114.5614 | G | 2638.6125 | 1319.8063 | 24 |
| 4 | 285.1543 | 143.1169 | G | 2581.5911 | 1291.2955 | 23 |
| 5 | 398.2403 | 199.6202 | L | 2524.5696 | 1262.7848 | 22 |
| 6 | 455.2535 | 228.1329 | G | 2411.4768 | 1206.2356 | 21 |
| 7 | 512.2833 | 256.6416 | G | 2354.4307 | 1177.7169 | 20 |
| 8 | 625.3673 | 313.1837 | L | 2297.4141 | 1149.2213 | 19 |
| 9 | 726.415 | 363.7075 | T | 2184.3586 | 1092.671 | 18 |
| 10 | 839.499 | 420.2495 | L | 2083.3108 | 1042.1554 | 17 |
| 11 | 910.5361 | 455.7681 | A | 1970.2205 | 985.6141 | 16 |
| 12 | 981.5732 | 491.2866 | A | 1899.1897 | 950.0835 | 15 |
| 13 | 1080.6417 | 540.8209 | V | 1828.1526 | 914.5763 | 14 |
| 14 | 1151.6788 | 576.3394 | A | 1729.0842 | 865.0421 | 13 |
| 15 | 1250.7472 | 625.8736 | V | 1658.0471 | 829.5236 | 12 |
| 16 | 1363.8313 | 682.4156 | L | 1558.9786 | 779.9893 | 11 |
| 17 | 1476.9153 | 738.9576 | I | 1445.8947 | 723.4473 | 10 |
| 18 | 1589.9994 | 795.4997 | L | 1332.8105 | 666.9053 | 9 |
| 19 | 1689.0677 | 845.0339 | V | 1219.7266 | 610.3633 | 8 |
| 20 | 1790.1155 | 895.5577 | T | 1120.6581 | 560.829 | 7 |
| 21 | 2131.3542 | 1066.1771 | C-Plamitoyol | 1019.6104 | 510.3052 | 6 |
| 22 | 2230.4229 | 1115.7114 | V | 678.3715 | 339.6858 | 5 |
| 23 | 2331.4705 | 1166.2352 | T | 579.3031 | 290.1516 | 4 |
| 24 | 2478.5059 | 1239.7529 | M-Oxidation | 478.2554 | 239.6277 | 3 |
| 25 | 2634.6069 | 1317.8035 | R | 331.22 | 166.11 | 2 |
| 26 | | | R | 175.1183 | 88.0595 | 1 |

**Supplementary Figure S22. MS spectra and table of mass shifts of S-acylation by LC-MS/MS.**

The left panel is the mass spectra of the peptide containing the S-acylation site, of which the abscissa is the mass-charge ratio (M/Z) and the ordinate is the ion peak intensity. The red is the detected y ion and the blue is the detected b ion. After the peptide fragments of proteins are broken under the action of energy, b ions and y ions will be produced, in which the N-terminal fragment is the b ion, and the C-terminal fragment is the y ion. The black peaks are the ion peaks detected by the instrument. The blue and red peaks are the ion peaks detected by the instrument and matched to the theoretical fragment ion peak generated by the fragmentation of the peptide. The blue and red peaks are the ion peaks detected by the instrument and matched with the black peak. The b ions and y ions correspond to each other, and the corresponding relationship is shown in the right panel. S-acylation modification occurs on CKST amino acids, for which the molecular weight change after modification is 238.23/266.26 Da (palmitic acid/stearic acid). The MS data were analyzed for protein modification using Proteome Discoverer 2.4.

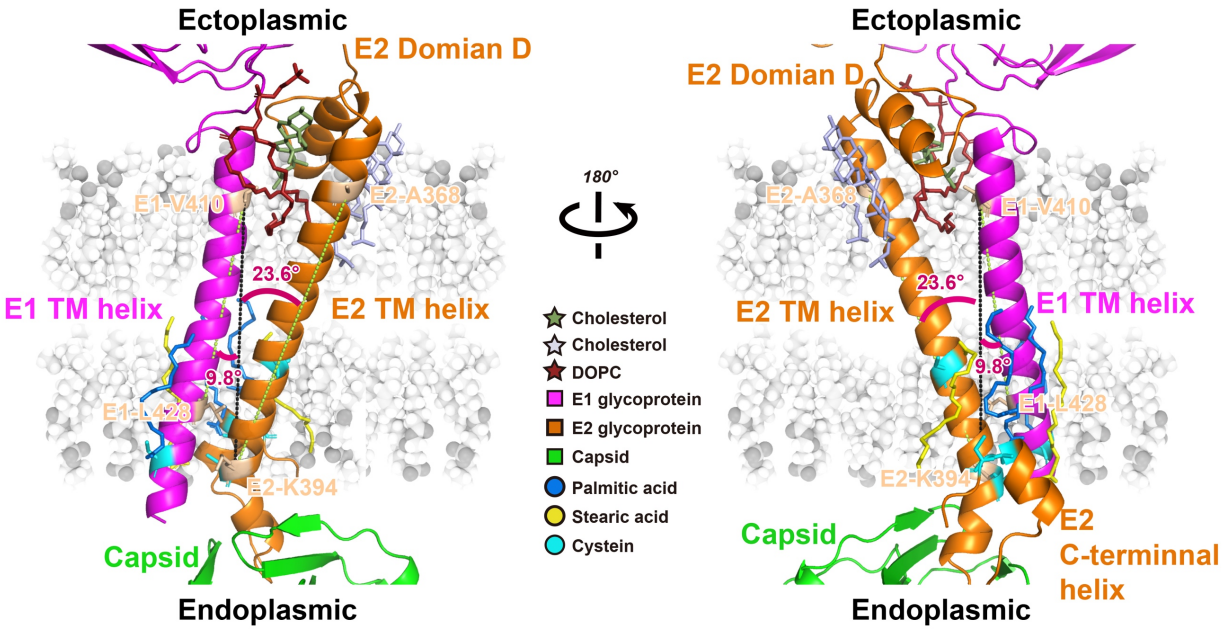


**Supplementary Figure S23. Transmembrane helices of E1 and E2.**

The black dash line between Cα of E1-V410 and E2-K394 is perpendicular to the lipid bilayer. The lime green dashes lines between Cα of E1-V410 and E1-L428, E2-A368 and E2-K394 are parallel to E1 and E2 helix, respectively. The angles between E1 and lipid bilayer, and the E2 and lipid bilayer are 9.8° and 23.6°, respectively. Residues E1-V410, E1-L428, E2-A368 and E2-K394 are shown as sticks and colored in wheat. Cholesterol, DOPC, cysteines, palmitic acids, and stearic acids are shown as sticks.

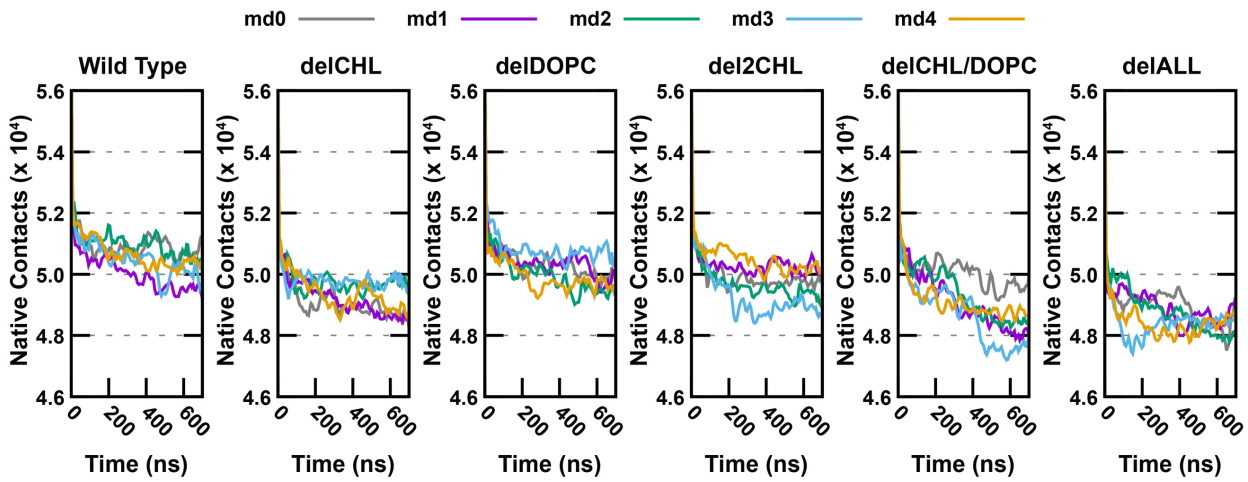


**Supplementary Figure S24. Time evolutions from MD simulation analyses for the native contacts within the E1-E2 complex.**

Time evolutions from MD simulation analysis for the number of native contacts of E1 (295-435) and E2 (269-422) for systems “Wild Type”, “delCHL”, “delDOPC”, “del2CHL”, “delCHL/DOPC”, and “delALL”. All curves were smoothed with the Bezier method and implemented in gnuplot.

**a**

| Virus | Protein | Sequence |
|---|---|---|
| GETV | E1 | NNQVFPDMSGTAMTWVQRVAGG |
| | E2 | PHEIILYYYGLYPAATIAAVSAA |
| SINV | E1 | DQEFQAAVSQTSWSWLFALFGG |
| | E2 | PHEIVQHYYHRHPVYTVMILVAA |
| MAYV | E1 | NGITLPDLSSTAMTWAQHLAGG |
| | E2 | PHEIIEYYYGLHPTTTIVVVVAV |
| VEEV | E1 | AQTFTAAVSKTAWTWLTSLLGG |
| | E2 | PHEVITHYYHRYPMSTILGLSIC |

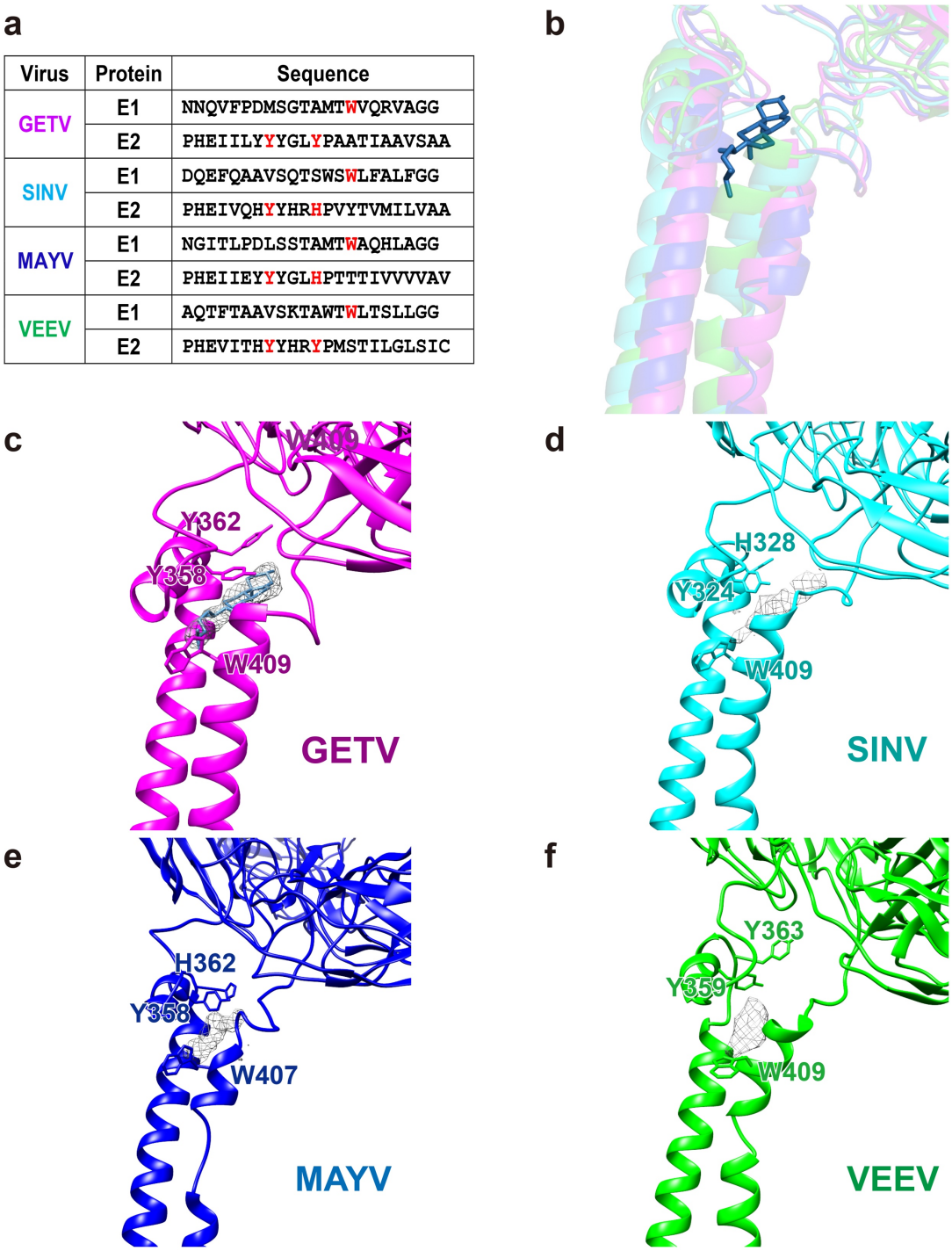


**Supplementary Figure S25. Comparison of the hydrophobic pocket structures between GETV and other alphaviruses.**

**a**, Table showing amino acid sequences of E1 and E2 helixes from GETV, SINV, MAYV, and VEEV. Residues involving cholesterol binding in the hydrophobic pocket are colored in red. **b**, Atomic models of GETV, SINV, MAYV, and VEEV are superimposed and

colored in magenta, cyan, marine, and green, respectively. **c** – **f**, Zoom-in views of the hydrophobic pocket in GETV, SINV, MAYV, and VEEV, with densities in the hydrophobic pocket shown as a mesh.

**Supplementary Table S1. Cryo-EM data collection and processing, block-based reconstruction, model building, and refinement statistics.**

| | | | |
|---|---|---|---|
| **Data Collection & Processing** | | | |
| Microscope | FEI Titan Krios | | |
| Camera | Gatan K3 | | |
| Magnification | 105K | | |
| Voltage(kV) | 300 | | |
| Total dose ($e^{-}$/Å$^2$) | 40 | | |
| Defocus range (μm) | 0.8-1.5 | | |
| Pixel size (Å/pixel) | 0.83 | | |
| Symmetry imposed | I3 | | |
| Movies (total) | 16,894 | | |
| Initial particles images | 171,059 | | |
| Final particles images | 100,226 | | |
| **Block-based Reconstruction** | | | |
| Block items | Clip1(5-fold) | Clip2(3-fold) | Clip3(2-fold) |
| Block symmetry imposed | C1 | | |
| Initial block images | 6,013,560 | | |
| Final block images | 2,041,957 | 2,446,428 | 2,889,370 |
| Final resolution (Å) | 2.81 | 2.92 | 2.85 |
| **Asymmetric Unit Model Building & Refinement** | | | |
| Initial model used (PDB code) | 3J0C | | |
| Composition | | | |
| Atoms | 32,620 | | |
| Residues | 4060 amino acids | | |
| Water | 0 | | |
| Ligand | STE, PLM, PCW, CLR, NAG, BMA, MAN | | |
| Bonds (RMSD) | | | |
| Length (Å) (# > 4σ) | 0.036 | | |
| Angles (°) (# > 4σ) | 2.021 | | |
| Clash score | 2.85 | | |
| Rotamer outliers (%) | 1.44 | | |
| Ramachandran plot (%) | | | |
| Outliers | 0.30 | | |
| Allowed | 2.80 | | |
| Favored | 96.90 | | |

**Supplementary Table S2. Interaction areas between GETV structural proteins.**

| | Interaction area, ($Å^2$) | $N_{HB}$ | $N_{SB}$ |
|---|---|---|---|
| **Interface 1** | 3319.1 | 34 | 2 |
| **Interface 2** | 568.9 | 5 | 0 |
| **Interface 3** | 107.0 | 1 | 1 |
| **Interface 4** | 594.9 | 5 | 1 |
| **Interface 5** | 523.2 | 9 | 1 |
| **Interface 6** | 444.4 | 2 | 0 |
| **Interface 7** | 163.6 | 2 | 2 |
| **Interface 8** | 599.1 | 4 | 3 |
| **Interface 9** | 367.1 | 5 | 1 |
| **Interface 10** | 341.0 | 2 | 1 |
| **Interface 11** | 185.6 | 1 | 0 |
| **Interface 12** | 91.7 | 1 | 2 |

interface areas, the number of hydrogen bonds ($N_{HB}$) and salt-bridges ($N_{SB}$) are listed in the table. The serial number of interfaces are illustrated in Figure S13.

**Supplementary Table S3. Protein-protein interactions in GETV and other alphaviruses**

| GETV | | | | Other Alphaviruses | | | | |
|---|---|---|---|---|---|---|---|---|
| **In the E1-E2-Capsid heterotrimer** | | | | | | | | |
| **Figure** | **Interaction** | **E2** | **E1** | **Alphavirus** | **Interaction** | **E2** | **E1** | **References** |
| Fig. 2B | HB | H226 | A92 | CHIKV | HB | H226 | A92 | Voss et al., 2010 [5] |
| | HB | S239 | S57 | CHIKV | HB | S239 | S57 | Voss et al., 2010 |
| | HB | R244 | P58 | CHIKV | HB | R244 | P58 | Voss et al., 2010 |
| | HB | Q247 | S66 | | | | | |
| | HB | S249 | V55 | | | | | |
| Fig. 2C | HB | R297 | A255 | MAYV | HB | R297 | A255, N252 | Ribeiro-Filho et al., 2021 [6] |
| | HB | G300 | F257 | CHIKV | HB | G301 | F257 | Voss et al., 2010 |
| | SB | R328 | D253 | | | | | |
| | HB | R336 | G258 | CHIKV | VDM | K337 | I387, N389 | Voss et al., 2010 |
| Fig. 2D | HB | W338 | V388 | CHIKV | HB | Y339 | V388 | Voss et al., 2010 |
| | HB | Q340 | S310, D385, H386 | CHIKV | SB | Q341 | S310, D385, H386 | Voss et al., 2010 |
| | HB | T342 | H386 | | | | | |
| Fig. 2E | HB | H348 | A361 | MAYV | HB | H348 | T403 | Ribeiro-Filho et al., 2021 |
| | HB | Y358 | V398 | | | | | |
| Fig. 2F | HB | S380 | T421 | | | | | |
| | HB | S384 | T421 | | | | | |
| **Figure** | **Interaction** | **E2** | **Capsid** | **Alphavirus** | **Interaction** | **E2** | **Capsid** | **References** |
| Fig. 2G | HB | A400 | K140 | | | | | |
| | HB | T402 | K140 | | | | | |
| **In the asymmetric unit** | | | | | | | | |
| **Figure** | **Interaction** | **E2** | **E2** | **Alphavirus** | **Interaction** | **E2** | **E2** | **References** |
| Fig. 3B | HB | Y18 | R144 | CHIKV | VDW | H18 | H142, S143, R144, P145, Q146 | Voss et al., 2010 |
| | HB | A20 | R144 | CHIKV | VDW | P20 | H142, S143, R144, | Voss et al., 2010 |

| | | | | | | | | |
|---|---|---|---|---|---|---|---|---|
| | | | | | | | P145, Q146 | |
| | SB | D21 | R144 | CHIKV | VDW | D21 | H142, S143, R144, P145, Q146 | Voss et al., 2010 |
| | SB | D24 | R94 | CHIKV | VDW | E24 | H142, S143, R144, P145, Q146 | Voss et al., 2010 |
| | HB | Q26 | R94 | CHIKV | VDW | H26 | H142, S143, R144, P145, Q146 | Voss et al., 2010 |
| | HB | Q128 | T142 | CHIKV | VDW | P128 | H142, S143, R144, P145, Q146 | Voss et al., 2010 |
| | HB | T142 | Q128 | CHIKV | VDW | H142 | H18, P20, D21, E24, G25, H26, S27, E109, T110, T126, P128, | Voss et al., 2010 |
| **Figure** | **Interaction** | **E2** | **E1** | **Alphavirus** | **Interaction** | **E2** | **E1** | **References** |
| Fig. 3C | HB | H287 | Y242 | CHIKV | VDW | Y288 | Q218, S234, Q235, A236, P237, | Voss et al., 2010 |
| **Figure** | **Interaction** | **E1** | **E1** | **Alphavirus** | **Interaction** | **E1** | **E1** | **References** |
| Fig. 3D | SB | K123 | E151 | CHIKV | VDW | R123 | N149, D151, H152 | Voss et al., 2010 |
| | HB | Y192 | E151, T153 | CHIKV | VDW | F192 | Y147 | Voss et al., 2010 |
| Fig. 3E | HB | T41 | N43 | SFV | HB | T41 | N43 | Roussel et al., 2006[7] |
| | HB | N43’ | T41’ | SFV | HB | N43 | T41 | Roussel et al., 2006 |
| **Figure** | **Interaction** | **Capsid** | **Capsid** | **Alphavirus** | **Interaction** | **Capsid** | **Capsid** | **References** |

| | | | | | | | | |
|---|---|---|---|---|---|---|---|---|
| Fig. 3F | HB | D120 | K151 | | | | | |
| | HB | K122 | D148 | | | | | |
| **Between two asymmetric units** | | | | | | | | |
| **Figure** | **Interaction** | **E1** | **E1** | **Alphavirus** | **Interaction** | **E1** | **E1** | **References** |
| Fig. 4B | HB, SB | E151 | K123, Y192 | CHIKV | VDW | D151 | R123, K176, P191, W192, G193, A194, Y214, R206 | Voss et al., 2010 |
| | HB | T153 | Y192 | CHIKV | VDW | A153 | W192, G193, A194 | Voss et al., 2010 |
| | HB | R160 | Y192 | | | | | |
| | HB | R160 | Y214 | | | | | |
| Fig. 4C | SB | R21 | D385 | SFV | SB | R21 | D284 | Roussel et al., 2006 |
| | HB | N22 | T307, P382 | CHIKV | VDW | P22 | T307, H381, P382, P383, R384 | Voss et al., 2010 |
| | SB | R289 | D311 | | | | | |
| Fig. 4D | SB | D323 | K351 | CHIKV | VDW | S323 | V315, I317, K319, E353 | Voss et al., 2010 |
| **Figure** | **Interaction** | **Capsid** | **Capsid** | **Alphavirus** | **Interaction** | **Capsid** | **Capsid** | **References** |
| Fig. 4E | HB | S180 | R244 | | | | | |
| | HB | Y185 | G205 | | | | | |
| | SB | R230 | E191 | | | | | |
| Fig. 4F | SB | E263 | K179 | | | | | |
| **Figure** | **Interaction** | **E2** | **E1** | **Alphavirus** | **Interaction** | **E2** | **E1** | **References** |
| Fig. 4G | HB | A417 | R437 | | | | | |

HB, Hydrogen bonds; SB, salt bridges; VDM, van der Waals contact.

Contacts were calculated using PISA[8].

Interactions highlighted in red represent the newly discovered interactions in the present study.

**Supplementary Table S4. Glycosylation sites in the E1 and E2 proteins**

| Protein | Glycosylation Type | Method | Glycosylation Site |
|---|---|---|---|
| E1 | O-Glycosylation | NetOGlyc[9] (www.cbs.dtu.dk/services/NetOGlyc/) | S250 |
| | | YinOYang[10] (www.cbs.dtu.dk/services/YinOYang/) | T53, **S66**, S104, T132, T144, S222, S226, T234, T288, S297, T368, S377, T435 |
| | | Previously reported | SINV S238 (no density)[6] |
| | | **Cryo-EM density (no atomic model)** | **S66** |
| | N-Glycosylation | NetNGlyc[10] (www.cbs.dtu.dk/services/NetNGlyc/) | N9, N22, N43, N100, N139, **N141,** N149, N175, N182, N186, N216, N252, N264, **N270**, N275, N298, **N335**, N395, N396. |
| | | GlycoMine[11] (glycomine.erc.monash.edu/Lab/GlycoMine/) | N9, N22, N43, N100, N139, **N141,** N149, N175, N182, N186, N216, N252, N264, **N270**, N275, N298, N395, N396. |
| | | **Mass spectrometry** | N9, N100, N139, **N141**, N149, N252, N264, **N270**, N275, N395, N396. |
| | | Previously reported | SINV N139, N245 (density, no atomic model) [12]<br>**CHIKV, MAYV N141 (atomic model)**[5,6] |
| | | **Cryo-EM density (no atomic model)** | **N335** |
| | | **Cryo-EM density (atomic model)** | **N141, N270** |
| E2 | O-Glycosylation | NetOGlyc | T142, T154, **T155**, T159, S160, S163. |
| | | YinOYang | T3, T87, S88, T122, S185, T211, S212, S213, T230, T238, S240, T261, **T264**, T343, T366. |
| | | Previously reported | N/A |
| | | **Cryo-EM density (no atomic model)** | **T155, T264** |
| | N-Glycosylation | NetNGlyc | N7, N33, N57, N65, N79, N187, **N200**, N207, N218, N231, **N262**, N332. |
| | | GlycoMine | N7, N57, N65, N79, N187, **N200**, N207, N218, N231, **N262**, N331, N332. |
| | | **Mass spectrometry** | N57, N187, **N200**, N218, N231, **N262**. |
| | | Previously reported | **CHIKV N196 (atomic model)**[5] |

| | | | |
|---|---|---|---|
| | | | **MAYV N262 (atomic model)**[6]<br>SINV N283 (density, no atomic model)[12] |
| | | **Cryo-EM density (atomic model)** | **N200, N262** |

**Supplementary Table S5. S-acylation sites in the E1 and E2 proteins**

| Protein | Acylation Type | Method | S-acylation Site |
|---|---|---|---|
| **E1** | S-acylation | CSS-Palm[13] (www.csspalm.biocuckoo.org/online.php) | C62, C63 |
| | | GPS-Palm[14] (gpspalm.biocuckoo.cn/) | C63, C259, **C433** |
| | | Mass spectrometry | C49, C62, C63, C68, C78, C94, C96, C114, C301, C306, C370, **C433** |
| | | Previously reported | BFV C436 (density, no atomic model)[15] |
| | | **Cryo-EM density (atomic model)** | **C433** |
| | N-acylation, O-acylation | Mass spectrometry | S136, T143 |
| | | Previously reported | N/A |
| | | **Cryo-EM density** | **N/A** |
| **E2** | S-acylation | CSS-Palm | C19, C22, **C415**, **C416** |
| | | GPS-Palm | **C385**, **C395**, **C415**, **C416** |
| | | Mass spectrometry | C19, C22, C28, C91, C105, C153, **C385**, **C395**, **C415**, **C416** |
| | | Previously reported | BFV C384, C387, C394, C414, C415 (density, no atomic model)[15]<br>VEEV C396, C416, C417 (density, no atomic model)[16] |
| | | **Cryo-EM density (atomic model)** | **C385, C395, C415, C416** |
| | N-acylation, O-acylation | Mass spectrometry | T130, T159, T171, K195, T196 |
| | | Previously reported | N/A |
| | | **Cryo-EM density** | **N/A** |

## References


1 Kumanomido, T. *et al.* Clinical and virological observations on swine experimentally infected with Getah virus. *Vet Microbiol* **16**, 295-301, doi:10.1016/0378-1135(88)90033-8 (1988).

2 Zhou, F. *et al.* Isolation and phylogenetic analysis of Getah virus from a commercial modified live vaccine against porcine reproductive and respiratory syndrome virus. *Mol Cell Probes* **53**, 101650, doi:10.1016/j.mcp.2020.101650 (2020).

3 Snyder, J. E. *et al.* Functional characterization of the alphavirus TF protein. *J Virol* **87**, 8511-8523, doi:10.1128/jvi.00449-13 (2013).

4 Zheng, S. Q. *et al.* MotionCor2: anisotropic correction of beam-induced motion for improved cryo-electron microscopy. *Nat Methods* **14**, 331-332, doi:10.1038/nmeth.4193 (2017).

5 Voss, J. E. *et al.* Glycoprotein organization of Chikungunya virus particles revealed by X-ray crystallography. *Nature* **468**, 709-712, doi:10.1038/nature09555 (2010).

6 Ribeiro-Filho, H. V. *et al.* Cryo-EM structure of the mature and infective Mayaro virus at 4.4 Å resolution reveals features of arthritogenic alphaviruses. *Nat Commun* **12**, 3038, doi:10.1038/s41467-021-23400-9 (2021).

7 Roussel, A. *et al.* Structure and interactions at the viral surface of the envelope protein E1 of Semliki Forest virus. *Structure* **14**, 75-86, doi:10.1016/j.str.2005.09.014 (2006).

8 Lawrence, M. C. & Colman, P. M. Shape complementarity at protein/protein interfaces. *J Mol Biol* **234**, 946-950, doi:10.1006/jmbi.1993.1648 (1993).

9 Steentoft, C. *et al.* Precision mapping of the human O-GalNAc glycoproteome through SimpleCell technology. *EMBO J* **32**, 1478-1488, doi:10.1038/emboj.2013.79 (2013).

10 Gupta, R. & Brunak, S. Prediction of glycosylation across the human proteome and the correlation to protein function. *Pac Symp Biocomput*, 310-322 (2002).

11 Li, F. *et al.* GlycoMine: a machine learning-based approach for predicting N-, C- and O-linked glycosylation in the human proteome. *Bioinformatics* **31**, 1411-1419, doi:10.1093/bioinformatics/btu852 (2015).

12 Chen, L. *et al.* Implication for alphavirus host-cell entry and assembly indicated by a 3.5Å resolution cryo-EM structure. *Nat Commun* **9**, 5326, doi:10.1038/s41467-018-07704-x (2018).

13 Ren, J. *et al.* CSS-Palm 2.0: an updated software for palmitoylation sites prediction. *Protein Eng Des Sel* **21**, 639-644, doi:10.1093/protein/gzn039 (2008).

14 Ning, W. *et al.* GPS-Palm: a deep learning-based graphic presentation system for the prediction of S-palmitoylation sites in proteins. *Brief Bioinform* **22**, 1836-1847, doi:10.1093/bib/bbaa038 (2021).

15 Kostyuchenko, V. A. *et al.* The structure of barmah forest virus as revealed by cryo-electron microscopy at a 6-angstrom resolution has detailed transmembrane protein architecture and interactions. *J Virol* **85**, 9327-9333, doi:10.1128/jvi.05015-11 (2011).

16 Zhang, R. *et al.* 4.4 Å cryo-EM structure of an enveloped alphavirus Venezuelan equine encephalitis virus. *EMBO J* **30**, 3854-3863, doi:10.1038/emboj.2011.261 (2011).